Timanian Fold-and-Thrust Belt and Caledonian Overprint in the Selis Ridge Imaged by New 3D Seismic Attributes and Spectral Decomposition

Jean-Baptiste P. Koehl [iD] [*1,2], **Israel Polonio**[2], **Luis A. Rojo-Moraleda**[3]

[1]Department of Earth and Planetary Sciences, McGill University, 3450 University Street, H3A 0E8, Montréal, Québec, Canada. | [2]Department of Geosciences, University of Oslo, Sem Sælands vei 1, 0371, Oslo, Norway. | [3]Aker BP Norge, Strandveien 13, 1366 Lysaker, Norway.

Abstract   The present study is a detailed structural analysis of 3D seismic data in the Selis Ridge in the western Loppa High in the Norwegian Barents Sea, to which seismic attributes and spectral decomposition were applied. The analysis reveals that pre-Devonian basement rocks are crosscut by a 40–50 kilometers wide, several kilometers thick, E–W- to WNW–ESE-striking fold-and-thrust belt, including a steep, kilometer-thick, top-SSW shear zone. The folds display dome- and trough-shaped geometries, the thrusts appear to have been reactivated dominantly as top-west structures, and the main shear zone warps over the top of the Selis Ridge. The fold-and-thrust belt is interpreted as part of the latest Neoproterozoic (ca. 650–550 Ma) Timanian Orogeny, which was reworked during E–W Caledonian contraction in the Ordovician–Silurian. The results are analogous to recent findings in the northern Norwegian Barents Sea and Svalbard. The presented interpretation provides the basis for discussing Neoproterozoic–Paleozoic plate tectonics reconstructions, the influence of Precambrian–early Paleozoic structures on post-Caledonian fault complexes, and the location of the Timanian and Caledonian suture zones.

Plain Language Summary   The contribution explores geophysical techniques to image the internal geometry of highly deformed rocks and crosscutting structures. The results show that the crust of the southwestern Barents Sea consists of E–W-trending, highly deformed belts of rocks that probably formed ca. 600 million years ago.

1   Introduction

The Norwegian Barents Sea is located along the paleo-Caledonian margin between Norway and Svalbard (1a) Despite a large number of studies focusing on the sub-surface geology of the southwestern Barents Sea (e.g., *Gudlaugsson et al.*, 1987, 1998; *Faleide et al.*, 1984, 1993; *Gabrielsen et al.*, 1990; *Indrevær et al.*, 2013; *Kairanov et al.*, 2021; *Marín et al.*, 2021), the Precambrian–early Paleozoic tectonic evolution of the area is still largely unknown. This is mostly due to the limitation of current seismic datasets, which do not image pre-Devonian basement rocks well (e.g., *Gudlaugsson et al.*, 1987; *Faleide et al.*, 1984, 1993; *Indrevær et al.*, 2013), and to the rarity of exploration wells penetrating basement rocks (*Slagstad et al.*, 2008). The nature of basement rocks in the Barents Sea and their evolution in the Precambrian–early Paleozoic therefore remain elusive.

Recently, the hydrocarbon industry took a new interest in pre-Devonian metamorphosed rocks after major oil discoveries were made in fractured Precambrian basement rocks in the North Sea (*Riber et al.*, 2015). In addition, oil discoveries in fractured–karstified Pennsylvanian–Permian carbonates over deformed basement rocks in the Loppa High in the Barents Sea (*Matapour et al.*, 2019) suggest there might be a relationship between basement-seated structures and the distribution of overlying karst systems and hydrocarbon accumulations. These discoveries highlight the important control of the state of deformation and nature of basement rocks on overlying sedimentary successions. In addition, the recent discovery of several kilometers thick, thousands of kilometers long Timanian thrust systems oblique to the N–S-trending Caledonian margin in the northern Barents Sea and Svalbard (*Klitzke et al.*, 2019; *Koehl*, 2020; *Koehl et al.*, 2022a) opened a new window into the early history of the Norwegian Arctic. These works suggest that Precambrian structural trends exist in basement rocks of the Barents Sea, and that these Precambrian trends can be segregated from other trends and mapped in detail.

The advancement of multi-attribute analysis techniques has significantly improved the ability to capture subtle geologic information that is not easily detected on the original seismic data or using single

*✉ jeanbaptiste.koehl@gmail.com
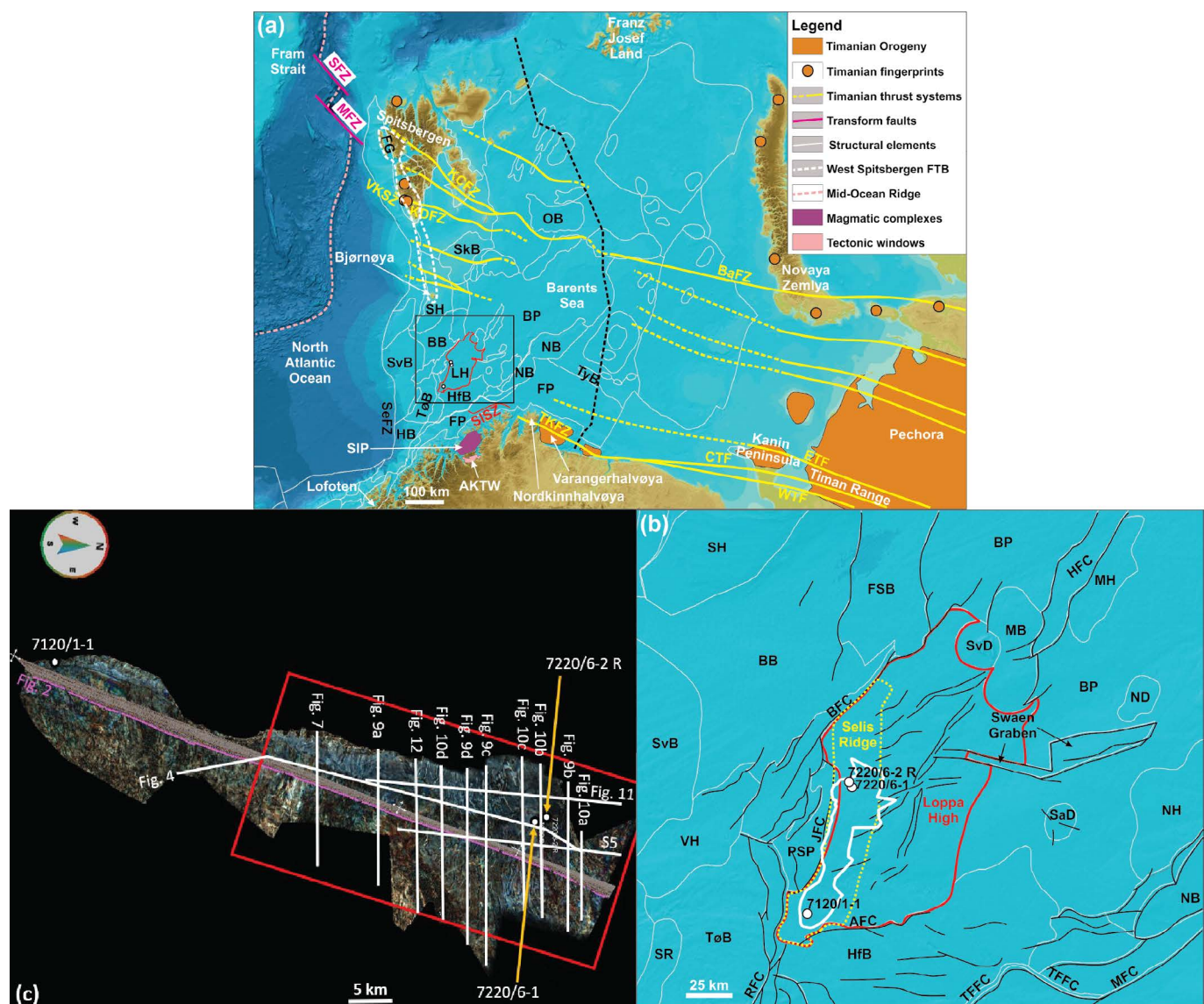
Figure 1 – **(a)** Overview map of the Barents Sea showing major structural elements in thin white lines (from the Norwegian Petroleum Directorate) and major fault trends in the Barents Sea (Timanian; yellow lines). **(b)** Zoom in the Loppa High and Selis Ridge showing the study area in the western Norwegian Barents Sea. The location of the 3D seismic dataset is shown as a thick white polygon. The basemap in **(a)** and **(b)** is from *Jakobsson et al.* (2012). **(c)** Color-blend map of the Top-basement reflection in the Selis Ridge. The location of Figure 8a–b is shown as a red rectangle, and seismic lines shown in subsequent figures as white lines. See location of dataset in **(b)**. Abbreviations: AFC: Asterias Fault Complex; AKTW: Alta–Kvænangen tectonic window; BaFZ: Baidaratsky Fault Zone; BB: Bjørnøya Basin; BFC: Bjørnøyrenna Fault Complex; BP: Bjarmeland Platform; CTF: Central Timan Fault; ETF: East Timan Fault; FG: Forlandsundet Graben; FP: Finnmark Platform; FSB: Fingerdjupet Sub-Basin; FTB: Fold-and-Thrust Belt; HB: Harstad Basin; HfB: Hammerfest Basin; HFC: Hoop Fault Complex; JFC: Jason Fault Complex; KCFZ: Kongsfjorden–Cowanodden fault zone; KDFZ: Kinnhøgda–Daudbjørnpynten fault zone; LH: Loppa High; MB: Maud Basin; MFC: Måsøy Fault Complex; MFZ: Molloy Fracture Zone; MH: Mercurius High; NB: Nordkapp Basin; ND: Norsel Dome; NH: Norsel High; OB: Olga Basin; PSP: Polhem Sub-Platform; RFC: Ringvassøya Fault Complex; SaD: Samson Dome; SeFZ: Senja Fracture Zone; SFZ: Spitsbergen Fracture Zone; SH: Stappen High; SIP: Seiland Igneous Province; SISZ: Sørøya–Ingøya shear zone; SkB: Sørkapp Basin; SR: Senja Ridge; SvB: Sørvestnaget Basin; SvD: Svalis Dome; TFFC: Troms–Finnmark Fault Complex; TKFZ: Trollfjorden–Komagelva Fault Zone; TyB: Tiddlybanken Basin; TøB: Tromsø Basin; VH: Veslemøy High; VKSZ: Vimsodden–Kosibapasset Shear Zone; WTF: West Timan Fault.

attributes. The present study utilizes post-stack re-processing, new seismic attributes and spectral de-composition on 3D seismic data in the western Loppa High (Figure 1a–b), where basement rocks are found at shallower level and form a N–S-trending ridge (Selis Ridge; *Sund et al.*, 1986; *Indrevær et al.*, 2017).

The presented results have implications for the nature of basement rocks in the Barents Sea, the

reworking of Timanian folds and thrusts by subsequent tectonic events, the accretion of the Barents Sea to Baltica, the location of the Timanian and Caledonian sutures (Figure 1a), and plate tectonic reconstructions of the Barents Sea in the Neoproterozoic–Phanerozoic.

More generally, the present study has significant implications for the interpretation of basement rocks

on seismic data and the geometry of fold-and-thrust belts worldwide, for structural inheritance in continental domains with more than one trend of preexisting structures, for petroleum exploration on basement highs, and for our understanding of craton growth and the stability of continental crust and tectonic plates over time. Notably, the 3D seismic attribute blend and spectral decomposition techniques used in the present study could be applied to other datasets to delineate basement structures and fabrics, and therefore significantly further correlation of structures and deformation events regionally. Improving the quality of regional seismic data is of great importance because, unlike fieldwork, they provide vertically- and laterally-continuous, several (tens–hundreds of) kilometers wide snapshots of the crust, which are invaluable in resolving regional geological relationships.

2 Geological Setting

2.1 Timanian Orogeny

The Timanian Orogeny is a latest Neoproterozoic (ca. 650–550 Ma) episode of top-SSW contraction that involved subduction beneath Baltica, traces of which are found in northwestern Russia (e.g., Novaya Zemlya, Pechora, Timan Range, Kanin Peninsula; *Siedlecka and Roberts*, 1995; *Olovyanishnikov et al.*, 2000; *Lorenz et al.*, 2004; *Roberts et al.*, 2004) and northeasternmost Norway (Varangerhalvøya; *Siedlecka and Siedlecki*, 1967, 1971; *Siedlecka*, 1975; *Gabrielsen et al.*, 2022, Figure 1a). This tectonic episode is associated with blueschist-facies metamorphism, top-SSW fold-and-thrust systems, and subduction- and island-arc-related magmatism in Russia (*Olovyanishnikov et al.*, 2000; *Gee et al.*, 2000; *Remizov*, 2003; *Dovzhikova et al.*, 2004; *Pease et al.*, 2004; *Beckholmen and Glodny*, 2004; *Remizov and Pease*, 2004; *Kostyuchenko et al.*, 2006). In Norway, Timanian deformation is characterized by mildly metamorphosed sedimentary successions truncated by the NNE-dipping Trollfjorden–Komagelva Fault Zone, which represents the Timanian front thrust in Varangerhalvøya (*Siedlecka and Siedlecki*, 1967; *Siedlecka*, 1975; *Herrevold et al.*, 2009; *Gabrielsen et al.*, 2022, Figure 1a).

Though previously thought to be restricted to northwestern Russia and northeasternmost Norway, other studies have shown that Timanian-aged igneous rocks (*Peucat et al.*, 1989; *Dallmeyer et al.*, 1990; *Griffin et al.*, 2012), (amphibolite-facies) metamorphism (*Manecki et al.*, 1998; *Majka et al.*, 2008, 2012) and associated unconformity (*Bjørnerud*, 1990; *Bjørnerud et al.*, 1991; *Birkenmajer*, 1991) are found in Svalbard (Figure 1a). Recent studies mapped and dated Timanian shear zones onshore Svalbard (e.g., Vimsodden–Kosibapasset Shear Zone; *Mazur et al.*, 2009; *Faehnrich et al.*, 2020), which connect with thousands of kilometers long, tens of kilometers thick systems of top-SSW brittle–ductile thrusts extend-

ing from the Urals to Svalbard (*Klitzke et al.*, 2019; *Koehl*, 2020; *Koehl et al.*, 2022a, Figure 1a). Moreover, studies in northern Greenland (*Rosa et al.*, 2016; *Estrada et al.*, 2018a) and Arctic Canada (*Estrada et al.*, 2018b), and in the Chukchi Borderland (*O'Brien et al.*, 2016) and the Lomonosov Ridge (*Rekant et al.*, 2019) reported respectively subduction-related magmatic suites of latest Neoproterozoic age and Timanian-aged igneous crust.

The timing of Timanian tectonism is constrained by geochronological studies of calc-alkaline and alkaline magmatic suites in northwestern Russia. Syn–late-subduction/collision calc-alkaline suites are dated to 700–515 Ma (*Dovzhikova et al.*, 2004; *Kuznetsov et al.*, 2007) and include 557 $\pm$ 6 Ma granitoids interpreted as late–post Timanian intrusions (*Gee et al.*, 2000; *Pease et al.*, 2004). By contrast, alkaline suites yielded ages of 565–500 Ma and display elongate shapes in the field believed to reflect intrusion in extensional–transtensional setting (*Larionov et al.*, 2004; *Kuznetsov et al.*, 2007).

2.2 Caledonian Orogeny

The Caledonian Orogeny resulted in the closure of the Iapetus Ocean and collision of Laurentia and Baltica in the Ordovician–Silurian. In northern Norway, the Berlevåg Formation (*Kirkland et al.*, 2007a) are part of the low-grade para-authochthonous cover and are in tectonic contact with structurally overlying rocks of the Kalak Nappe Complex (*Roberts*, 1998), which are believed to be of Iapetian–Laurentian origin (*Slagstad et al.*, 2006; *Corfu et al.*, 2007; *Kirkland et al.*, 2007b, 2008). The latter were intruded by igneous rocks of the Seiland Igneous Province in the latest Neoproterozoic–earliest Cambrian and thrust onto Baltica and metamorphosed to amphibolite facies during the Caledonian Orogeny (*Sturt et al.*, 1978; *Gayer et al.*, 1985).

In Svalbard, Caledonian deformation is recorded as several–tens of kilometers wide fold-and-thrust belts including blueschist–eclogite-facies metamorphism (*Horsfield*, 1972; *Manby*, 1986; *Ohta et al.*, 1989, 1995; *Dallmeyer et al.*, 1990; *Harland et al.*, 1992; *Gee et al.*, 1994; *Witt-Nilsson et al.*, 1998; *Johansson et al.*, 2004, 2005). Caledonian metamorphism and magmatism are recorded as far east as Franz Joseph Land (*Knudsen et al.*, 2019) and Severnaya Zemlya (*Kurapov et al.*, 2020). Since Svalbard was until recently thought to have been assembled and accreted to Norway during the Caledonian Orogeny, the Caledonian suture was therefore proposed to run NE–SW through the Barents Sea (*Breivik et al.*, 2005; *Knudsen et al.*, 2019). However, the recent discovery of continuous, latest Neoproterozoic Timanian thrusts extending from northwestern Russia to Svalbard challenges this claim and rather suggests a location of the Caledonian suture west of or in western Svalbard (*Koehl et al.*, 2022a).

Caledonian thrusts show an overall top-SE transport direction onshore northern Norway (*Ramsay*

et al., 1985; *Townsend et al.*, 1986; *Gayer et al.*, 1987; *Townsend*, 1987; *Kirkland et al.*, 2007a) and on the western Finnmark Platform in the Barents Sea (*Johansen et al.*, 1994; *Gudlaugsson et al.*, 1998; *Koehl et al.*, 2018), but strike N–S in Svalbard (*Horsfield*, 1972; *Birkenmajer*, 1975, 2004; *Harland*, 1978; *Manby*, 1986; *Ohta et al.*, 1989; *Dallmeyer et al.*, 1990; *Harland et al.*, 1992; *Gee and Page*, 1994; *Gee et al.*, 1994; *Lyberis and Manby*, 1999; *Johansson et al.*, 2004, 2005) and the northern Barents Sea (*Koehl et al.*, 2022a). The northerly swing of Caledonian fabrics and structures occurs on the Finnmark Platform and can be traced on high-resolution magnetic and gravimetric data (*Gernigon and Brönner*, 2012; *Gernigon et al.*, 2014, Figure 1a).

2.3 Late–post-Caledonian Extensional Collapse

In Devonian times, late–post Caledonian collapse-related extension triggered reactivation of Caledonian thrusts and shear zones as low-angle normal faults, leading to the formation of core complexes on-shore northern Norway (e.g., *Steltenpohl et al.*, 2011) and northwestern Svalbard (*Braathen et al.*, 2018), and on the Finnmark Platform in the Barents Sea (*Koehl et al.*, 2018, Figure 1a). Extensional collapse is recorded by up to ca. 9–10 km thick sedimentary deposits in northern Spitsbergen (*Murascov and Mokin*, 1979; *Friend et al.*, 1997). A Late Devonian episode of contraction, the Svalbardian Orogeny, was previously inferred (*Vogt*, 1928; *Vogt and Horn*, 1941; *Roberts*, 1983; *Torsvik et al.*, 1986; *Piepjohn*, 2000), but was later firmly rejected in Norway (e.g., *Hossack*, 1984; *Norton*, 1987; *Chauvet and Séranne*, 1994) and is now thought to be unlikely to have occurred in Svalbard either (*Koehl and Allaart*, 2021; *Koehl et al.*, 2022b, and references therein)).

In the Carboniferous, continued extension triggered high-angle brittle faulting and formation of grabens and half grabens filled with sedimentary successions, which are preserved in Svalbard (*Cutbill and Challinor*, 1965; *Cutbill et al.*, 1976; *Aakvik*, 1981; *Gjelberg*, 1984; *Braathen et al.*, 2011), and in the northern (*Anell et al.*, 2016; *Klitzke et al.*, 2019; *Koehl et al.*, 2022a) and southern Barents Sea (*Indrevær et al.*, 2017; *Koehl et al.*, 2018; *Tonstad*, 2018). Conversely, areas located in the footwall of normal faults (e.g., Jason Fault Complex; *Indrevær et al.*, 2017, 2018) were uplifted, e.g., Selis Ridge in the western Loppa High (Figure 1b), and show thinning, onlapping, (partly) eroded or non-deposited upper Paleozoic sedimentary successions (*Sund et al.*, 1986; *Indrevær et al.*, 2017). In the Pennsylvanian–Permian, extension gradually died out and a regional carbonate platform developed in the Barents Sea (*Samuelsberg et al.*, 2003; *Larssen*, 2005; *Rafaelsen et al.*, 2008; *Nordaunet-Olsen et al.*, 2015) and Svalbard (*Cutbill and Challinor*, 1965; *Ahlborn and Stemmerik*, 2015).

2.4 Late Jurassic–Early Cretaceous Rifting

The Triassic was tectonically quiet despite local occurrences of minor normal faulting in the Barents Sea and Svalbard (*Anell et al.*, 2013; *Osmundsen et al.*, 2014; *Ogata et al.*, 2018). The Jurassic–Cretaceous, however, recorded renewed extension, which resulted in the formation of rift basins filled with several kilometers thick sedimentary successions in the western Barents Sea (*Gudlaugsson et al.*, 1987; *Faleide et al.*, 1984, 1993; *Gabrielsen et al.*, 1990; *Indrevær et al.*, 2013; *Kairanov et al.*, 2021; *Marín et al.*, 2021).

In the Loppa High, the Selis Ridge was uplifted during down-west normal movement along the Jason Fault Complex (*Gabrielsen et al.*, 1990; *Indrevær et al.*, 2017, 2018), down-northwest movement along the Bjørnøyrenna Fault Complex in the north (*Rønnevik and Jacobsen*, 1984; *Gabrielsen et al.*, 1990, 1997), and down-south normal movement along the Asterias Fault Complex in the south (*Gabrielsen*, 1984; *Gabrielsen et al.*, 1984, 1990, Figure 1b). Note that the latter possibly acted as a reverse fault in the Triassic and Early Cretaceous (*Gabrielsen et al.*, 2011; *Indrevær et al.*, 2017). Mini basins such as the Swaen Graben, consists of WNW–ESE- and ENE–WSW-trending segments (Figure 1b), formed east of the Selis Ridge (*Gabrielsen et al.*, 1990; *Omosanya et al.*, 2017). The basin terminates against N–S- to NNE–SSW-striking faults just east of the Selis Ridge (*Gabrielsen et al.*, 1990; *Indrevær et al.*, 2017, Figure 1b).

2.5 Early Cenozoic Eurekan Contraction

In the early Cenozoic, opening of the Labrador Sea and Baffin Bay led to the collision of northern Greenland with western Svalbard during the Eurekan tectonic event (*Chalmers and Pulvertaft*, 2001; *Oakey and Chalmers*, 2012), which resulted in the formation of the West Spitsbergen Fold-and-Thrust Belt (*Steel et al.*, 1985; *Dallmann et al.*, 1993, Figure 1a). This deformation belt continues into the northern Barents Sea and was believed to terminate just north of Bjørnøya (*Nøttvedt et al.*, 1988; *Bergh and Grogan*, 2003). However, traces of post-Permian contraction onshore Bjørnøya, including N–S-trending folds and reverse faults (*Worsley et al.*, 2001, and Koehl's personal observations) suggest that Eurekan tectonism reached farther south.

In the southern Barents Sea, this is illustrated by reactivation of the Bjørnøyrenna and Jason fault complexes as reverse faults, possibly starting in the Late Cretaceous–early Cenozoic (*Gabrielsen et al.*, 1997; *Indrevær et al.*, 2017). This was potentially accompanied by large-scale transpressional movements along the Senja Fracture Zone during the opening of the North Atlantic (*Riis et al.*, 1986; *Knutsen et al.*, 1992; *Knutsen and Larsen*, 1997, Figure 1a) as suggested by NW–SE contractional folds and thrusts in the Sørvestnaget Basin (*Kristensen et al.*, 2018).

2.6 Mid–late Cenozoic Extension

The breakup of the North Atlantic initiated at the Paleocene–Eocene boundary (*Storey et al.*, 2007; *Faleide et al.*, 2008) and was followed by breakup in the Fram Strait at magnetic chron 6 in the early Miocene (*Dumais et al.*, 2020, Figure 1a). Extension resulted in normal faulting and sediment deposition in basins, such as the Forlandsundet Graben in western Spitsbergen (*Manby*, 1986; *Lepvrier*, 1990; *Kleinspehn and Teyssier*, 1992, 2016; *Schaaf et al.*, 2021), and the Sørvestnaget and Tromsø basins in the southwestern Barents Sea (*Rønnevik and Jacobsen*, 1984; *Gabrielsen et al.*, 1990; *Knutsen and Larsen*, 1997, Figure 1a). Cenozoic uplift resulted in thinned Cenozoic and Quaternary sedimentary successions in the Loppa High (*Knutsen et al.*, 1992; *Knutsen and Larsen*, 1997).

3 Data and Methods

The results we present are based on detailed analysis and interpretation of high-resolution 3D seismic reflection data from Lundin Energy Norway imaging the Selis Ridge. Spectral decomposition techniques and several seismic attributes were applied to the 3D seismic data to remove noise and enhance the visualization and mapping of intra-basement structural trends. Interpretation of intra-basement reflections and structures was also enhanced by using time-slices through the frequency spectral decomposition volume (Figure 1c). Post-stack reprocessing included structural smoothing, integrated trace, frequency, and filtering helped to enhance the signal-to-noise ratio of the 3D seismic data. The seismic volume was cut at a depth of 3.5 seconds (TWT).

Both amplitude (amplitude, variance, correlation mapping, continuity) and volumetric attributes (apparent structural dip and azimuth, curvature, flexure, envelope, tensor) were applied to the data. For example, the curvature attribute improves imaging of geometric features at various scales. The structural dip attribute is an edge detection method which enhances rapid changes in local dip, e.g., fractures and bedding surfaces. Seismic flexure has the potential to delineate subtle faults and fractures, especially those overlooked by the popular discontinuity and curvature attributes, and the envelope attribute delineate faults by lateral discontinuity. We used opacity blend to visualize the blending of the selected attributes.

The present work focuses on Precambrian–lower Paleozoic rocks in the Selis Ridge, which consists of four segments (southernmost, southern, central, and northern; Figure 2) characterized by seismic reflections grouped into discrete seismic facies (SF; Figure 3). Notably, the southern and northern segments are dominated by reflections of SF1 and SF3, the southernmost and central segments by SF2 reflections, and the boundary between the southernmost and southern and the central and northern segments by SF4 reflections (Figure 3).

Post-Caledonian sedimentary successions are therefore neither interpreted, nor discussed. Post-Caledonian brittle faults are exclusively described where interacting with underlying basement reflections. For more details about their formation and reactivation history, the reader is referred to previous works (*Gabrielsen*, 1984; *Rønnevik and Jacobsen*, 1984; *Gabrielsen et al.*, 1984, 1990; *Indrevær et al.*, 2017, 2018). Our interpretation is tied to exploration wells 7120/1-1, 7220/6-1 and 7220/6-2R, all of which penetrated metamorphosed basement rocks in the Selis Ridge (Figure 1).

4 Results and Interpretations

The Selis Ridge is located in the western part of the Loppa High, where it defines an elongated N–S-trending ridge of uplifted pre-Devonian basement rocks. It is bounded from the Hammerfest Basin by the Asterias Fault Complex in the south, from the Polhem Sub-Platform by the Jason Fault Complex in the west, and from the Bjørnøya Basin by the Bjørnøyrenna Fault Complex in the northwest (Figure 1b). The Selis Ridge is divided into northern, central, southern and southernmost segments, which are respectively dominated by moderate- to high-, low-, moderate-, and low- to moderate-amplitude reflections (Figure 2). Both the central and southernmost segments become narrower upwards (dome shape), whereas the southern and northern segments become broader upwards (trough shape; Figure 2). Internal reflections in all four segments are abruptly truncated upwards by post-Caledonian sedimentary successions.

4.1 Folded Basement Rocks

4.1.1 Descriptions

In the north, basement reflections dominantly dip steeply to the south and show high amplitude (seismic facies 1 – SF1; Figure 3). Southwards, basement reflections display a gradual decrease in amplitude and show low amplitude in the southern segment. They also show a gradual change in dip direction towards the central segment, where they dominantly dip northwards (Figure 4). In the central segment of the Selis Ridge, the seismic facies is characterized by a partly chaotic signature as shown by the relatively homogeneous, low-amplitude, and poor lateral and vertical continuity of seismic reflections in this area (SF2; Figure 3). Seismic reflections in the southern segment abruptly switch to a steep northerly dip and moderate amplitude (Figure 5). In the southernmost segment, reflections display moderate amplitude and a gentle northerly dip or partly chaotic character (Figure 5).

Reflections in the northern segment show dominantly asymmetric, both convex- and concave-upwards curving geometries from several hundreds of meters to several kilometers wide (SF1; Figure 6a–e). In the central, southern and southernmost segments, both asymmetric and symmetric curvy ge-
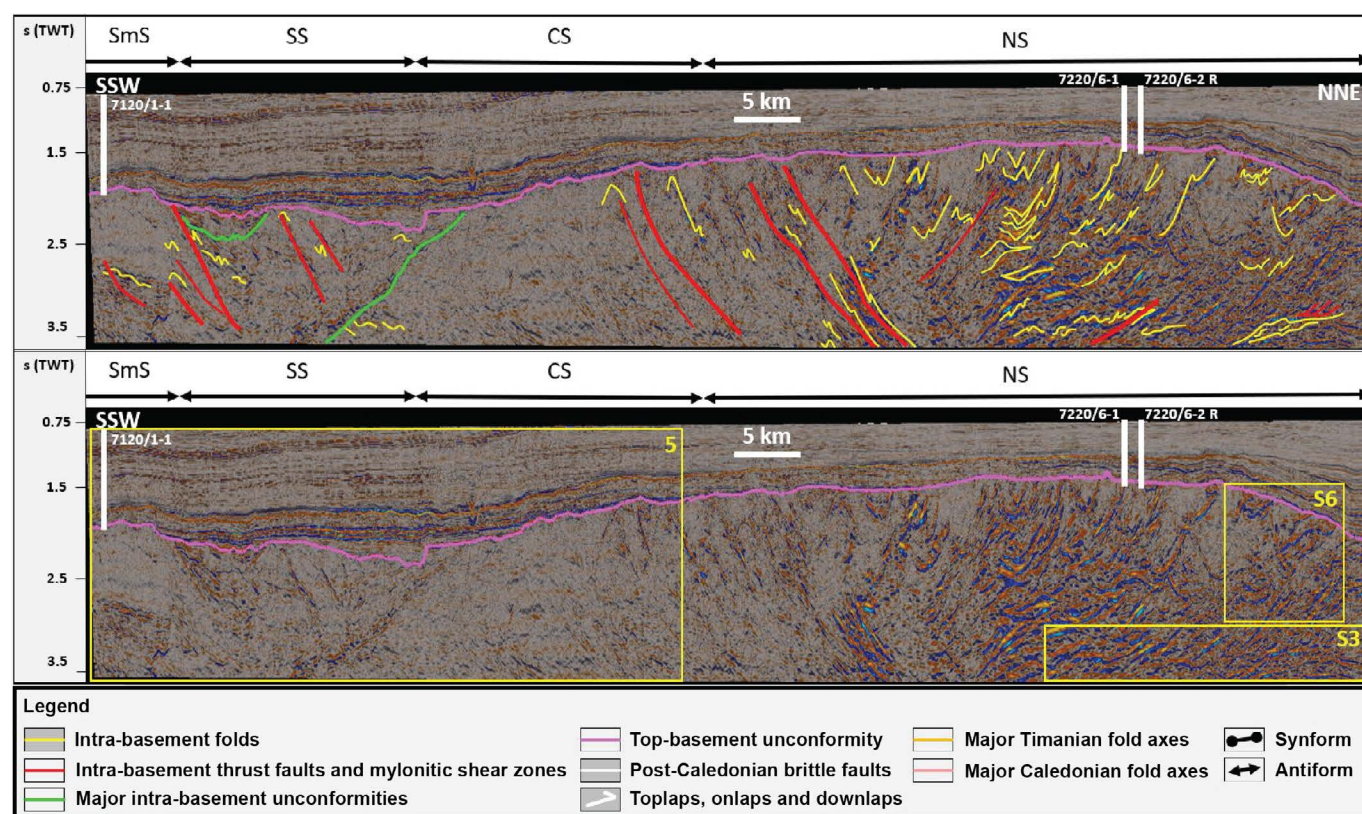
Figure 2 – Interpreted (upper inset) and uninterpreted (lower inset) seismic section through the Selis Ridge showing a major E–W- to WNW–ESE-trending fold-and-thrust belt including dominantly top-north asymmetric folds and top-south to top-SSW major thrusts and mylonitic shear zones. Notice the trough-shaped (half-graben-like) geometries defined by the northern and southern segments, whereas the southernmost and central segments display dome (horst-like) geometries. The lateral projections of exploration wells 7120/1-1, 7220/6-1 and 7220/6-2 R are shown in as white lines. Yellow rectangles show the location of Figure 5, and Figures SI-3 and SI-6 (see Supporting Information). The legend is common to all seismic sections. Location is shown in Figure 1c. Abbreviations: CS: Central segment; NS: Northern segment; SmS: Southernmost segment; SS: Southern segment.

ometries are found, both in N–S and E–W seismic transects, though in minor numbers due to the lower amplitude of reflections in these areas (SF2; Figures 7 and Figure SI-1 in Supporting Information).
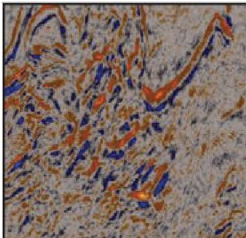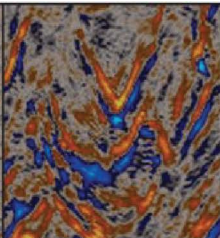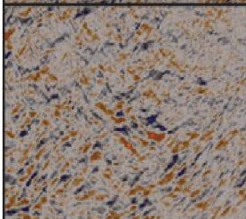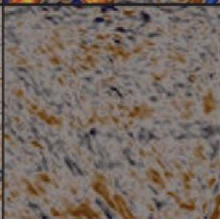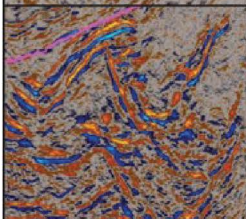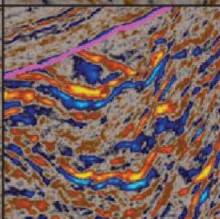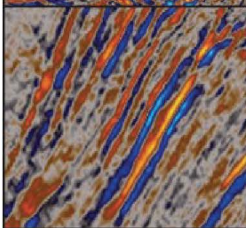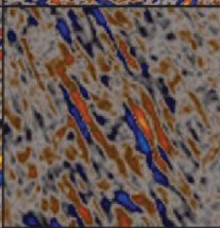
In the north, several kilometers wide, asymmetric curvy reflections commonly display acute angles and show wavelengths of several kilometers (Figure 6d–e). In places, reflections curve sideways into pointy recumbent packages (Figure 6d–e). In map view, the reflections that are part of these packages form kilometer-scale oval-shaped geometries with an E–W-trending long axis (Figure 8 and Figure SI-2 in Supporting Information).

SF1 asymmetric curvy geometries are also observed at scales of several hundreds of meters to 1–2 km. In the north, the convex-upwards endmember of these features consistently shows long southern and short northern edges, whereas the concave-upwards endmember displays long northern and short southern edges (Figure 4). Both end members geometries appear to lean towards the north in the northern segment (Figure 6d–e). By contrast, convex-upwards asymmetric reflections farther south (near the central segment) display long northern and short southern edges and lean towards the south (Figure 6a–c). This is also the case locally in the central, south-

ern and southwesternmost segments (Figures 2 and 5). In E–W cross section, comparable asymmetric geometries are observed and consistently display long eastern and short western edges leaning towards the west (Figure 9a–d). Like every other intra-basement reflection, asymmetric curvy geometries are truncated upwards by the main post-Caledonian unconformity (Figures 2 and 4). In places, SF1 asymmetric curvy reflections are found in clusters and appear arranged into 0.5–1 second (TWT) thick packages of S-shaped reflections (Figures 9b–d and 10a, and Figure SI-3 in Supporting Information).

The (eastern portion of) the northern and central segments and the southern segment of the Selis Ridge display (several) kilometer-wide, 0.5–1.5 second (TWT) thick, U-shaped packages of low- to high-amplitude seismic reflections (SF3; Figure 3) respectively in E–W and N–S cross sections (Figures 5, 9a–d, and 10b–c). The U-shaped packages of SF3 are separated from underlying packages of tighter (i.e., forming acute angle) curving SF1 reflections by major high-amplitude reflections, which truncate underlying reflections at a high angle and against which overlying reflections terminate as downlaps (Figures 9b–d and 10b–c). By contrast to other commonly curving intra-basement reflections forming acute angles,

Figure 3 – Summary table of all the seismic facies observed in the study area. Seismic facies 1 and 4 were penetrated respectively by exploration wells 7220/6-1 and 7220/6-2 R in the northern segment of the Selis Ridge (see also Figure SI-1 in Supporting Information), and seismic facies 2 was penetrated by exploration well 7120/1-1 in the southernmost segment.
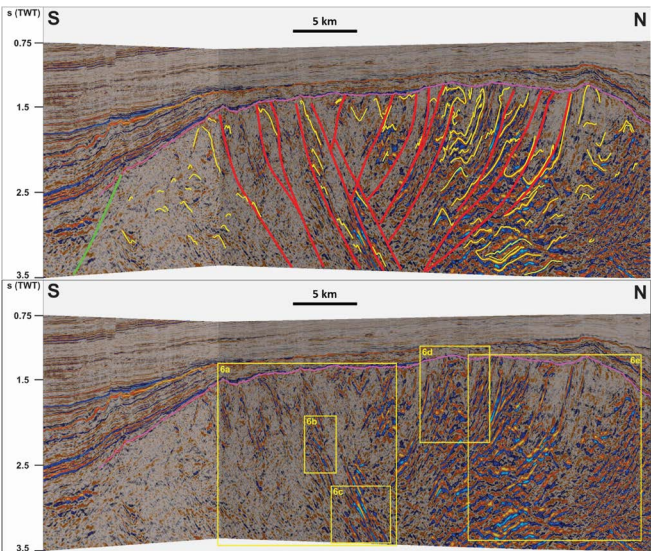
Figure 4 – Interpreted (upper inset) and uninterpreted (lower inset) seismic section through the northern and central segments of the Selis Ridge. In the northern segment, the section shows asymmetric folds and major thrusts and shear zones with dominant top-north tectonic transport direction in the north and top-south transport in the south. In the central segment, the section shows upright folds. The location of Figure 6a–e is shown as yellow rectangles. See legend in Figure 2. Location is shown in Figure 1c.
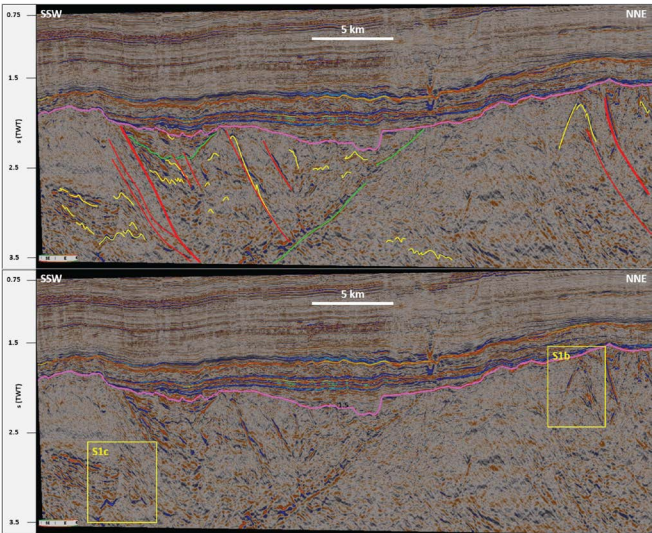
Figure 5 – Interpreted (upper inset) and uninterpreted (lower inset) seismic section through the central, southern and southernmost segments of the Selis Ridge. The section shows upright folds within the dome-shaped central and southernmost segments, and top-south thrusts and a U-shaped basin in the trough-shaped southern segment. The location of Figure SI-1(b-c) is shown as yellow rectangles. See Figure 2 for location and legend.
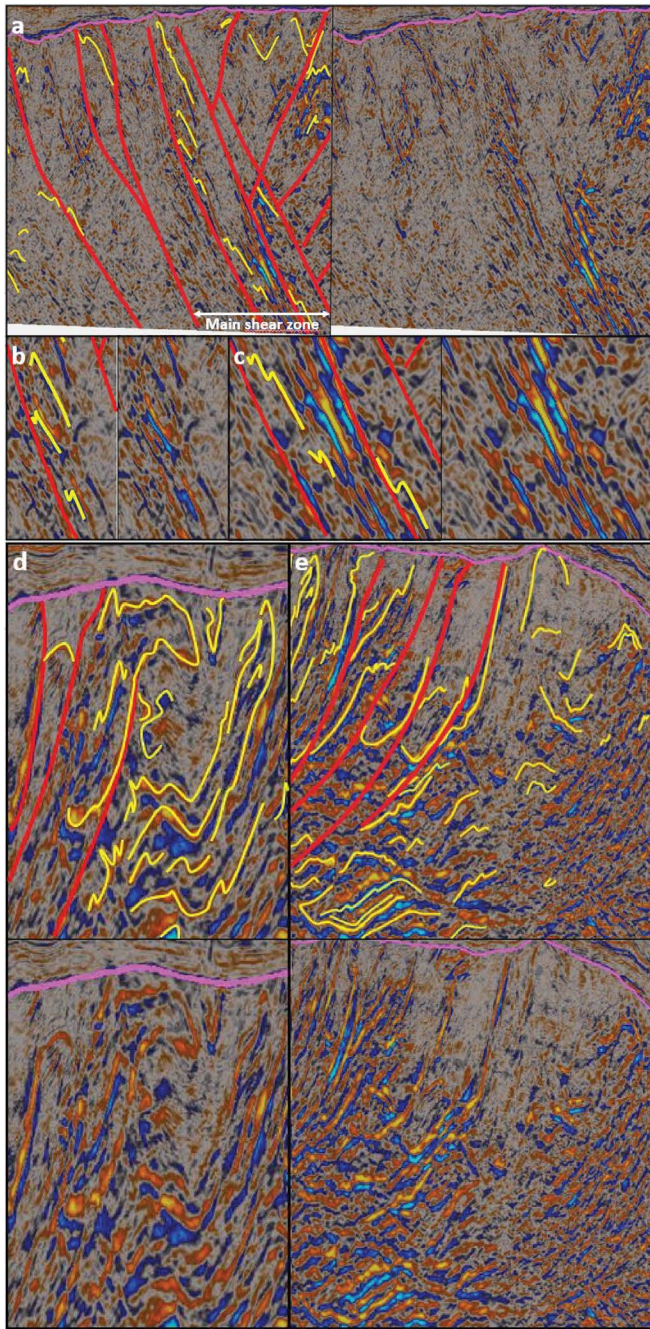
Figure 6 – (a) Interpreted (left hand-side inset) and un-interpreted (right hand-side inset) showing the main NNE-dipping shear zone at the boundary between the northern and the central segments of the Selis Ridge. The main zone consists dominantly of NNE-dipping mylonitic thrusts and asymmetric, south- to SSW-verging folds indicating top-SSW tectonic transport. **(b)** and **(c)** show interpreted (left hand-side inset) and uninterpreted (right hand-side inset) zoomed-in portions of the main shear zone and asymmetric, south- to SSW-verging fold structures. **(d)** Interpreted (upper inset) and uninterpreted (lower inset) showing recumbent, isoclinal folds, including an overturned antiform near the Top-basement reflection. **(e)** Interpreted (upper inset) and uninterpreted (lower inset) displaying thrusts accompanied by overlying (ramp) antiforms and underlying synforms. In the north, the data show symmetrical upright fold structures. Location of (a–e) is shown in Figure 4. See legend in Figure 2
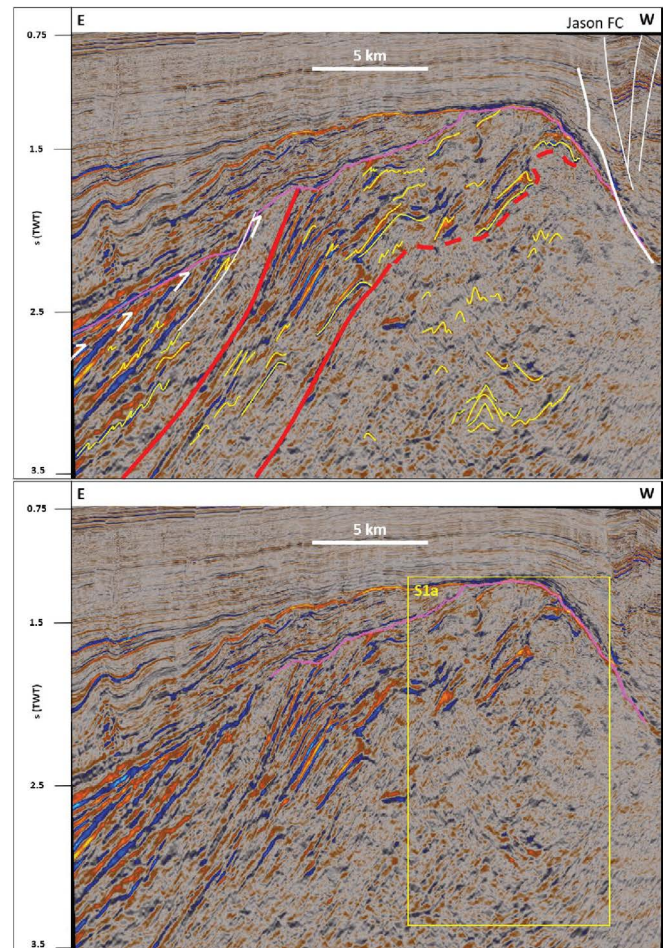
Figure 7 – Interpreted (upper inset) and uninterpreted (lower inset) seismic section through the main NNE-dipping shear zone. Notice how the shear zone, which involves slightly asymmetric west-verging folds, warps over the top of the Selis Ridge and begins to curve down on the western flank of the ridge where it is truncated by the Jason Fault Complex. Meta-igneous rocks in the footwall of the shear zone show dominantly upright folds. Also note the exploitative attitude of post-Caledonian brittle faults in the east, which formed along preexisting low-angle basement fabrics. The yellow rectangle shows the location of a. See legend in Figure 2 and location in Figure 1c.

SF3 reflections within these upper packages typically undulate forming curving geometry with obtuse angles and show exclusively concave-upwards geometries (Figures 5, 9b–d, and 10b–c). In map view, all the SF3 U-shaped packages display oval-shaped geometries (Figure 8).

4.1.2 Interpretations

On the one hand, the pervasive low-amplitude, partly chaotic character of SF2 reflections in the central and southernmost segments suggest relatively homogeneous rock units with little lithological variations. These basement rocks are therefore interpreted as foliated igneous rocks (Figure 3). This is supported by penetration of foliated mafic metaigneous rocks (fine-grained gabbro/basalt?) by exploration well 7120/1-1 in the southernmost segment of the Selis Ridge (cf. completion report of well 7120/1-
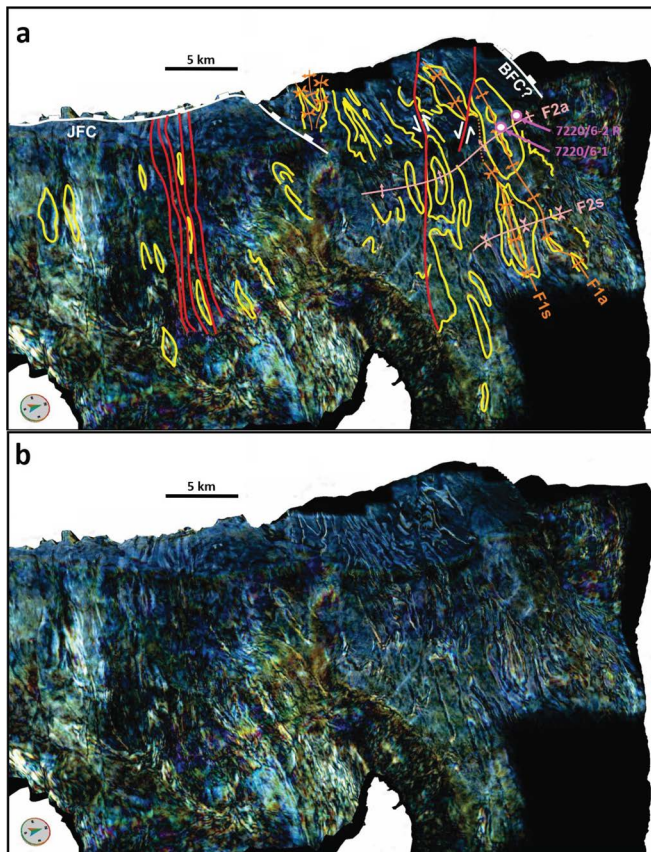
Figure 8 – **(a)** Interpreted and **(b)** uninterpreted zoom in the northern segment of the Selis Ridge showing the oval shape of fold structures in basement rocks (yellow lines) with elongated E–W-trending axes (orange lines; e.g., folds F1a and F1s) and flattened N–S-trending axis (pink lines; e.g., folds F2a and F2s). The main NNE-dipping shear zone is shown in red and post-Caledonian brittle fault complexes in white. Notice the highly flattened and stretched fold structures within the main shear zone. Location is shown in Figure 1c.

1 at npd.no) and by petrological modelling suggesting the presence of large intermediate–mafic intrusions in the southern part of the Loppa High (*Fichler and Pastore*, 2022). On the other hand, the high-amplitude character of SF1 reflections in the northern and southern segments suggests frequent and significant lithological variations in basement rocks there. Thus, rocks in the northern and southern portions of the Selis Ridge are interpreted as several kilometers thick successions of metasedimentary (possibly with metaigneous/metavolcanic) rocks (Figure 3). This is supported by exploration well 7220/6-1 and 7220/6-2R, which penetrated quartzite and phyllite and phyllonite in the northern segment (see Section SI-1, Figures SI-4A and SI-4B in Supporting Information).

The curvy geometries of SF1 and SF2 reflections are interpreted as fold structures, and these compare well with folds in metamorphosed basement rocks on seismic data elsewhere (e.g., *Ji and Long*, 2006; *Koehl and Allaart*, 2021; *Koehl et al.*, 2022a). The wavelength of fold structures ranges from hundreds of meters to several kilometers with amplitudes of a few tens to hundreds of milliseconds (TWT) and trend domi-

nantly E–W and subsidiarily N–S (Figures 4 and 9a–d). Notable geometries include dominantly (1) hundreds of meter- to kilometer-wide, west-, north- and south-verging, close to tight folds (Figure 4) arranged into duplexes and/or antiformal thrust stack structures (Figure 10a and d, and Figures SI-3 and SI-5 in Supporting Information; *Boyer and Elliott*, 1982), (2) several kilometers wide, isoclinal, recumbent synclines and (ramp) anticlines (Figure 6d–e), and (3) open upright folds in the northernmost tip and central, southern and southernmost segments (Figures 5 and 6e, and Figure SI-6 in Supporting Information). The oval shapes formed by several kilometers wide folds in map view are interpreted as non-cylindrical dome-shaped folds (Figure 8). This is reflected by the interaction of west-verging N–S- and south- and north-verging E–W-trending folds (Figures 2, 4, 6a–e, 7, 9a–d, and 10a–d, and Figure SI-6 in Supporting Information). Fold structures are tighter on N–S-trending seismic sections (Figures 2, 4, and 6a–e) than on E–W-trending transects (Figures 7, 9a–d, and 10a–d). This is further illustrated by the short N–S axes and elongated E–W axes of the oval-shaped in map view (Figure 8).

The shallow U-shaped packages (SF3) in the eastern part of the central and northern segments and in the southern segment of the ridge (Figures 5, 9b–d, and 10b–c) are consistently located above major disruption surfaces and display gently curved instead of moderately–tightly curved geometries. In addition, they are involved in oval-shaped folds (troughs) in map view (Figure 8). They are therefore interpreted as potential piggyback basins (Figure 3). This is further supported by the downlap geometries of reflections within these packages and by the truncation of underlying, more tightly folded U-shaped reflections, suggesting deposition within an evolving basin (Figures 9b–d and 10b–c).

4.2 Faults and Mylonitic Shear Zones in Basement Rocks

4.2.1 Descriptions

In the northern and southern segments of the Selis Ridge, moderate- to high-amplitude SF1 reflections are commonly truncated by steep, planar, dominantly high-amplitude, south-dipping, disruptive surfaces (SF4; Figure 3), which terminate abruptly against the post-Caledonian unconformity upwards (Figure 6d). The upwards terminations of these disruption surfaces commonly coincide with minor (tens of meters high) protuberances in the trace of the post-Caledonian unconformity (Figures 5, and 6a and d–e). It should be noted that concave-upwards reflections defining synforms are consistently found below major SF4 disruptions, whereas dominantly convex-upwards geometries interpreted as antiforms are generally found above (Figure 6d–e).

In the east in the central and northern segments, moderate- to high-amplitude SF1 and SF2 reflections are truncated by similarly steep, planar and high-
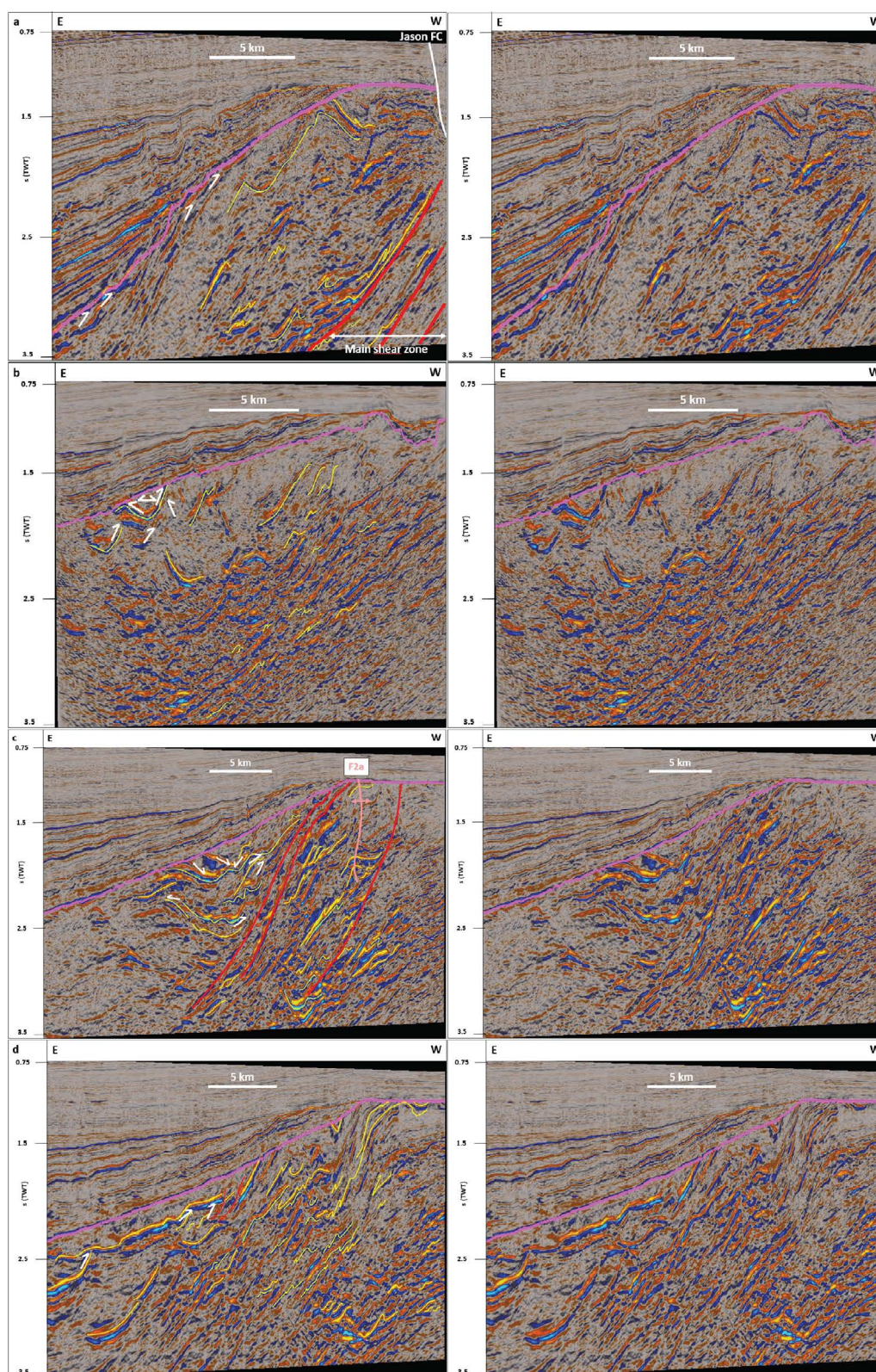
Figure 9 – Interpreted (left hand-side inset) and uninterpreted (right hand-side inset) E–W seismic sections through the northern segment of the Selis Ridge. **(a)** The section shows the eastward component of dip of the main shear zone. Notice the generally more open character of west-verging folds in basement rocks compared to south- to SSW-verging folds in N–S-trending sections, apart from a few isoclinal folds in the vicinity of the shear zone. **(b)** West-verging folds, S-shaped duplexes, and potential U-shaped piggyback basin in basement rocks. The section shows toplap reflection geometries below the base of the piggyback basin and the Top-basement unconformity, and onlap to downlap geometries within the piggyback basin. **(c)** Section showing a major U-shaped piggyback basin in the hanging wall of major top-west thrusts, which are associate with west-verging folds and duplex structures. Notice the downlap and toplap geometries respectively within and below the basin. The section also shows the southern continuation of fold F2a, which displays a geometry of ramp anticline (Caledonian antiform; see also Figure 8 for map view of the fold). **(d)** West-verging folds and piggyback basin with associated toplap refection terminations. Notice the coinciding of more gently dipping basement fabrics and flattening of the Top-basement unconformity in the west. Location of insets is shown in Figure 1c and legend in Figure 2.
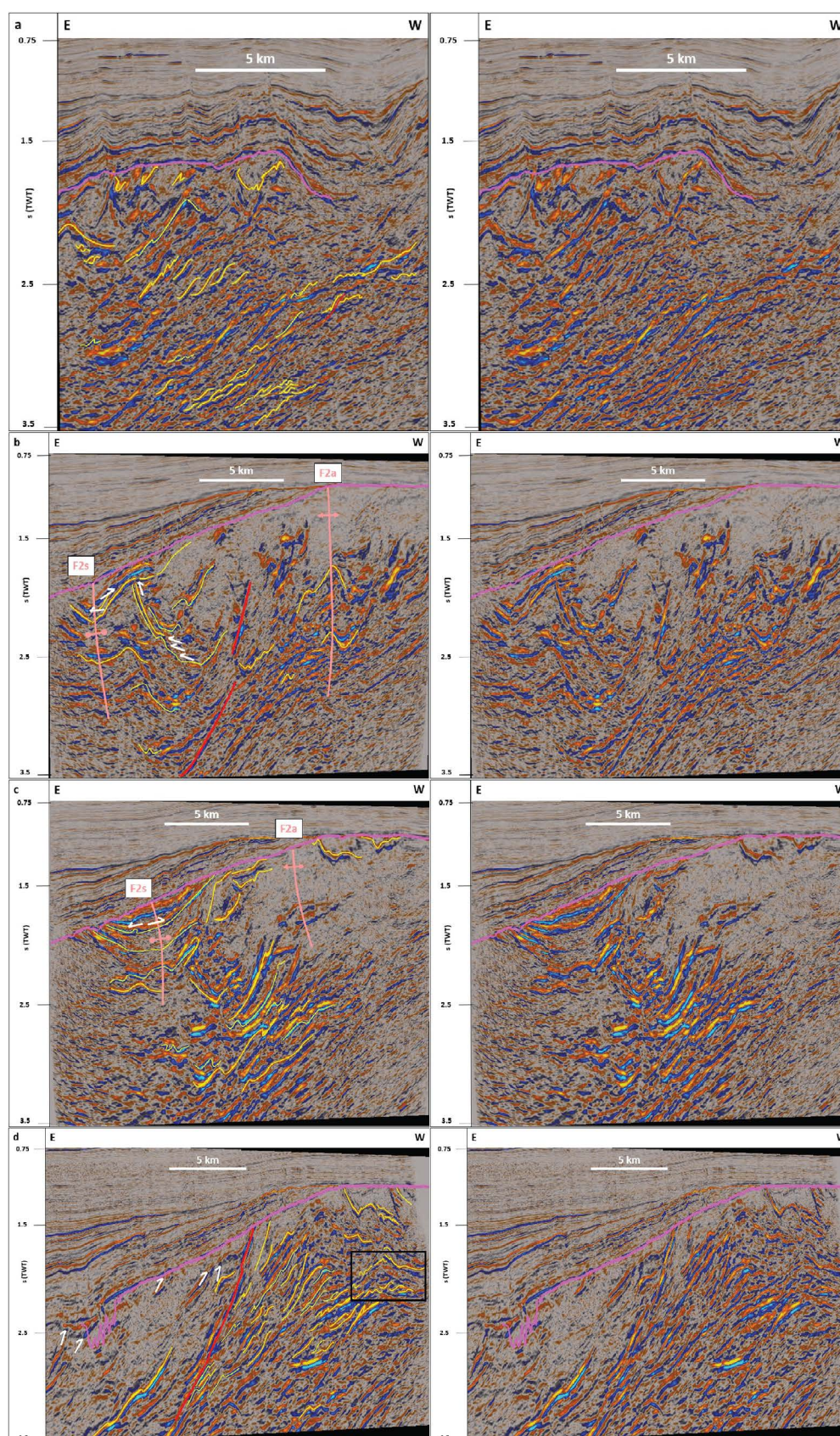
Figure 10 – Interpreted (left hand-side inset) and uninterpreted (right hand-side inset) E–W seismic sections through the northern segment of the Selis Ridge. **(a)** West-verging folds and duplexes (S-shaped) in the northernmost Selis Ridge. **(b)** and **(c)** U-shaped piggyback basins with toplap truncation of seismic reflections by the base of overlying basins. Notice the onlap geometries within the basins. The section also shows Caledonian folds F2s and F2a, which coincide respectively with U-shaped piggyback basins and with shallower portions of the Selis Ridge where piggyback basins are missing. **(d)** Antiformal thrust stack in the northern segment of the Selis Ridge(black frame). Note the antiformal geometry defined by basement fabrics in the west, which coincides with the shallowest portion of the ridge and with the flat portion of the Top-basement unconformity. Location of insets is shown in Figure 1c and legend in Figure 2.

amplitude, semi-continuous, east-dipping disruptive surfaces (Figure 9a and c). These disruptions, however, do not truncate the shallowest U-shaped reflection packages in the east, which are located above major disruption surfaces (Figure 10b–c).

An item of notable importance is found at the boundary of the central and northern segments (Figures 2, 4, and 8) and corresponds to a 4–5 km wide package of steep (see Figure SI-7, in Supporting Information, for depth conversion of the structure dip angle), planar, north-dipping, moderate- to high-amplitude reflections (SF4; Figure 3), which coincides with an E–W- to WNW–ESE-trending magnetic lineament (Gernigon et al., 2014). Reflections within this package are more continuous and consistently truncate less steeply dipping reflections in the north and south (Figure 6a). Within this package, multiple, hundreds of meter- to kilometer-wide, upwards-convex reflections with short southern and long northern edges leaning towards the south are found above major disruption surfaces in N–S-trending cross sections (Figure 6b–c). In E–W-trending cross sections, the package of SF4 reflections displays an overall upwards-convex, steeply east-dipping geometry that becomes gently dipping to sub-horizontal near the top of basement rocks in the western part of the Selis Ridge (Figures 7 and 9a). Major linear north- and east-dipping continuous reflections within this package truncate other reflections below the main post-Caledonian unconformity. Notably, all gently to moderately south-dipping SF1 reflections in the north are truncated (Figure 4). The north- and east-dipping geometries of the SF4 reflections indicate an overall north-northeastern dip (Figures 6a–c, 7, and 9a), and depth conversion suggests a gentle to moderate dip (31–46°; Figure SI-7 in Supporting Information).

An analogous feature is observed at the boundary of the southern and southernmost segments of the Selis Ridge. There, a kilometer-wide package of steeply north-dipping, moderate-amplitude SF4 reflections abruptly truncates less steeply dipping moderate- to high-amplitude SF1 reflections in the north, including reflections part of the U-shaped SF3 package (Figure 5). Depth conversion suggests a moderate dip angle (41–46°; Figure SI-7 in Supporting Information).

4.2.2 Interpretations

SF1–3 fold structures in the Selis Ridge are truncated by steep east-, north- and south-dipping, planar, dominantly high-amplitude SF4 reflections. Because of their disruptive and high-amplitude character, steep planar SF4 reflections are interpreted as faults with possible fault-parallel dykes (Figure 3). The small (tens of meters high) positive relief created by these faults (and possible fault-parallel dykes) on the morphology of the main post-Caledonian unconformity suggest that they consist of material more resistant to erosion than the surrounding bedrock. A possible candidate is mylonite, which is made up

with denser, strongly deformed material (*Bell and Etheridge*, 1973; *Sibson*, 1977; *Arbaret and Burg*, 2003). A major argument to support this interpretation is the higher reflectivity character (higher amplitude) and planar aspect of mylonite and tilted dykes on seismic data generated respectively by preferred mineral orientation along foliation and shear surfaces (*Christensen*, 1965, 1966; *Fountain et al.*, 1984; *Hurich et al.*, 1985) and by density contrast of igneous rocks (especially if mafic) with adjacent mylonite and metasedimentary rocks (e.g., *Phillips et al.*, 2018; *Koehl et al.*, 2018, 2022a). Positive relief is commonly created by mineral precipitation along shear zones and magmatic intrusions more resistant to erosion (e.g., *Eberts et al.*, 2021, their Figure 2b), which typically produces rugose subcrops with numerous asperities and protuberances (e.g., *Phillips et al.*, 2016, 2018, their Figures 14 and 1c, respectively). In addition to their ductile character, it is highly probable that the faults are (at least) partly brittle as suggested by their disruptive and offsetting character. One of the high-amplitude SF4 reflections interpreted as a mylonitic ductile fault surface was penetrated by exploration well 7220/6-2R in the northern part of the Selis Ridge (see Figure 1 for location, Section SI-1, Figures SI-4A and SI-4B in Supporting Information). Cores from the well showed that basement rocks consist of foliated metasedimentary rocks alternating with cataclastic and foliated fault rocks, including possible phyllonite, cataclasite, and mylonite (see Section SI-1, Figures SI-4A and SI-4B in Supporting Information). This strongly supports an interpretation as brittle–ductile mylonitic faults/shear zones and suggests the presence of a major, 40–50 km wide, E-W-trending fold-and-thrust system (with north- and south-verging folds) in basement rocks in the Selis Ridge and of a less developed, 10–20 km wide system of top-west folds and thrusts. Seismic data only extend to 3.5 seconds (TWT) depth and it is possible that the fold-and-thrust system extends beyond that depth. Nevertheless, based on seismic velocities of ca. 6–7 km.s^{-1} for Precambrian–lower Paleozoic basement rocks in the Barents Sea (*Gernigon et al.*, 2018), it appears that fold-and-thrust systems in the Selis Ridge are at least several to tens of kilometers thick (Figures 1, 4, 7, 9a-b, and 10a-d).

SF4 mylonitic ductile faults (and possibly related intrusions) alternate with and truncate packages of basement rocks deformed into hundreds of meters to several kilometers wide west-, south- and north-verging fold structures (SF1). Notably, several kilometers wide, E–W-trending, isoclinal, recumbent synclinal folds are consistently found below major fault disruption surfaces, and comparable (ramp) anticlines are consistently located above major faults (Figure 6d–e). These E–W-trending, (several) kilometers wide anticlines and synclines and the major, WNW–ESE-striking faults are therefore interpreted as thrusts and contractional, thrust-related folds. Furthermore, the truncation and (tens to hundreds of meter-scale) lateral offset of fold axial surfaces by

major E–W-striking faults in map view suggest a minor component of (dominantly left-) lateral movement along WNW–ESE-striking faults in the Selis Ridge (i.e., reverse-sinistral oblique slip; Figure 8).

As a result, the 4–5 km wide package of steep, NNE-dipping, planar, high-amplitude SF4 reflections bounding the central segment from the northern segment is interpreted as a major, WNW–ESE-striking, brittle–ductile, oblique-slip shear zone with possible shear-zone-parallel dykes (Figure 6a). This is further supported by the gentle to moderate dip angle of the structure based on depth conversion (31–46°; Figure SI-7 in Supporting Information). The contractional origin of the shear zone is inferred from the presence of south-verging folds in between major shear surfaces (and possible intrusions), which indicate a formation as a top-SSW thrust (Figure 6b–c). A similar interpretation is also proposed for the kilometer-wide package of moderate-amplitude SF4 reflections separating the southern segment from the southernmost segment (Figure 5). These two major shear zones in the Selis Ridge are comparable in thickness and geometry to other major shear zones on seismic data elsewhere (*Christensen and Szymanski*, 1988; *Fisher et al.*, 1989; *Wang et al.*, 1989; *Johansen et al.*, 1994; *Hajnal et al.*, 1996; *Gudlaugsson et al.*, 1998; *Phillips et al.*, 2016; *Hedin et al.*, 2016; *Fazli Khani et al.*, 2017; *Clerc et al.*, 2018; *Koehl et al.*, 2018; *Lenhart et al.*, 2019; *Phillips and McCaffrey*, 2019; *Osagiede et al.*, 2020; *Wrona et al.*, 2020).

4.3 Faults and Folds in post-Caledonian Sedimentary Rocks

4.3.1 Descriptions

Bjørnøyrenna Fault Complex   Brittle faults in post-Caledonian sedimentary rocks include parts of the Bjørnøyrenna and the Jason fault complexes (Figures 1b and 8). The Bjørnøyrenna Fault Complex (*Rønnevik and Jacobsen*, 1984; *Gabrielsen et al.*, 1990, 1997) displays a major, ca. 0.5 second (TWT), down-north normal offset of the main post-Caledonian unconformity. Upwards, it shows decreasing normal offset prior to dying out within Triassic sedimentary rocks (Figure 11), which are folded into an anticline. Folding along the Bjørnøyrenna Fault Complex and in adjacent upper Paleozoic–lower Cenozoic, post-Caledonian sedimentary successions is truncated by the late Cenozoic Upper Regional Unconformity. The fault dies out eastwards (Figures 2 and 4).

At depth, the Bjørnøyrenna Fault Complex flattens so that it becomes parallel to the base of and bedding surfaces within Carboniferous–Permian sedimentary successions, possibly creating a décollement above the top of underlying basement rocks. At deeper levels, below the basin, the fault merges with moderately north-dipping, high-amplitude SF1 basement reflections making up the northern limb of a major antiform at the northern end of the Selis Ridge (Figure 11). Below the adjacent post-Caledonian sedimentary basin, SF1 reflections are involved in a sev-
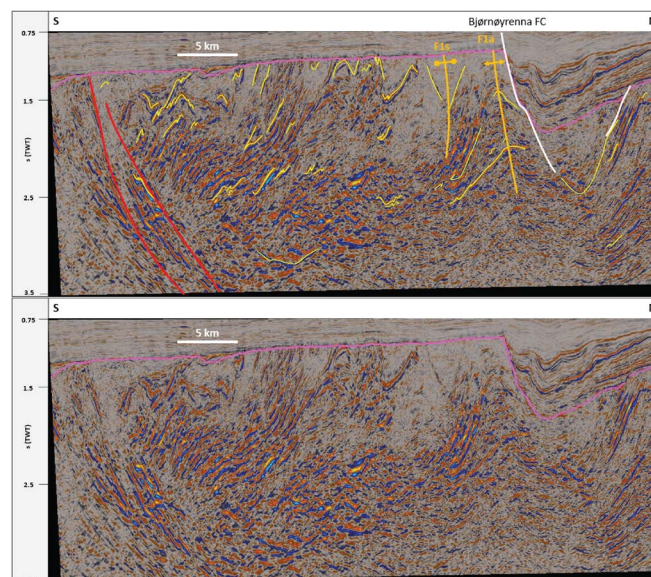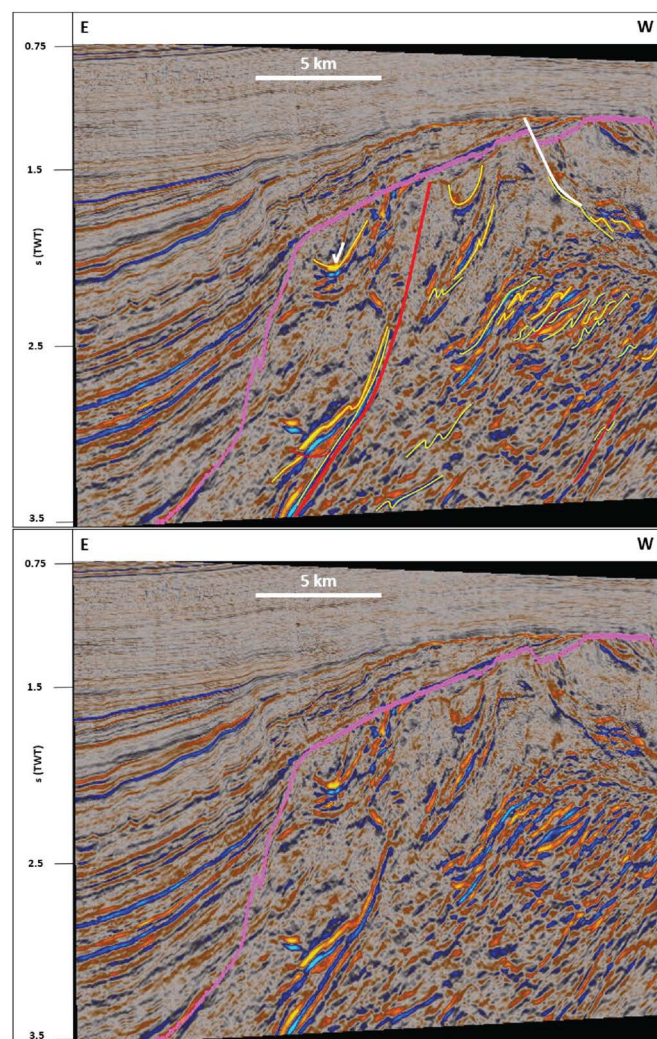

Figure 11 – Interpreted (upper inset) and uninterpreted (lower inset) throught the northern segment of the Selis Ridge. The section shows the main NNE-dipping shear zone in the south, north-verging folds in the hanging wall of the shear zone, and the axial traces of the F1a and F1s folds (see also Figure 8 for map view). The section also shows the influence of basement fabrics on post-Caledonian faults and basins. Faults developed on fold limbs (e.g., Bjørnøyrenna Fault Complex) and basins coincide with major synformal folds in basement rocks. Location is shown in Figure 1c and legend in Figure 2.

eral kilometers wide synform (probable syncline), which mimics the attitude of the trough-shaped basin. On the northern end of the basin, minor, moderately south-dipping, normal faults antithetic to the Bjørnøyrenna Fault Complex offset the main post-Caledonian unconformity and merge with underlying moderately south-dipping, high-amplitude SF1 (SF4?) reflections within basement rocks making up the northern limb of the synform (Figure 11).

Jason Fault Complex   The Jason Fault Complex (*Indrevær et al.*, 2017, 2018) and a possibly related minor fault are partly observed along the southwestern part of the Selis Ridge (Figures 7 and 12). There, the Jason Fault Complex is associated to minor N–S folds and subvertical reverse faults within post-Caledonian sedimentary successions (Figure 7). At depth, the Jason Fault Complex parallels and merges with the western limb of a major, several kilometers wide, N–S-trending antiform within basement rocks (Figure 7).

Farther north, a small brittle fault offsets the post-Caledonian unconformity and basement rocks along the limb of the next major, N–S-trending antiform (Figure 12). The fault shows a thin wedge of thickened, upper Paleozoic sedimentary strata in the hanging wall and merges with the west-dipping fold limb at depth (Figure 12).

In the east, the post-Caledonian unconformity is offset by minor, moderately east-dipping normal faults (Figure 7). These faults die out rapidly upwards

Figure 12 – Interpreted (upper inset) and uninterpreted (lower inset) E–W seismic section through the northern segment of the Selis Ridge. The section shows a U-shaped piggyback basin in the hanging wall of a major top-west thrust and west-verging folds and duplexes in the footwall in the core of the ridge. The data also show how preexisting basement fabrics was partly reactivated during post-Caledonian normal faulting (segment of the Jason Fault Complex formed along west-dipping fold limb). Location is shown in Figure 1c and legend in Figure 2.

at or near the base of the post-Caledonian sedimentary successions.

4.3.2 Interpretations

The parallel and merging attitude of the Bjørnøyrenna and Jason fault complexes and related faults with major fold limbs in basement rocks at depth suggest that post-Caledonian faults and basins developed along preexisting N–S and E–W basement-seated structures, in the present case, several kilometers wide synforms and antiforms (Figures 7, 11, and 12). By contrast, the minor, moderately dipping normal faults in the north and east merge with underlying high-amplitude SF1 and/or SF4 mylonitic basement reflections (Figure 11). They show an exploitative relationship (*Phillips et al.*, 2016) and are therefore interpreted as reactivated

embrittled portions of mylonitic thrusts/shear zones.

There seem to be no relationship between folds in upper Paleozoic–lower Cenozoic sedimentary rocks and along the Bjørnøyrenna and Jason fault complexes and folds in basement rocks (see discussion chapter). The folds in post-Caledonian rocks are interpreted as fault-propagation folds (*Suppe and Medwedeff*, 1990), which suggest inversion of the faults. These folds are truncated by the (late Cenozoic) Upper Regional Unconformity (Figure SI-8 in Supporting Information), which suggests that the formation of the folds and inversion of related faults (Bjørnøyrenna and Jason fault complexes) most likely took place in the Late Cretaceous–early Cenozoic.

5 Discussion

5.1 Crosscutting Relationships

N–S fold and thrust structures within basement rocks in the Selis Ridge display typical dips and geometries for contractional structures, thus supporting our interpretation and suggesting that they were not or only mildly reworked during subsequent events. The tighter and more evolved character of E–W folds and thrusts suggest that they formed first and were subsequently reworked (refolded) during the formation of the N–S-trending fold-and-thrust system. A probable scenario would therefore involve a first episode of N–S-oriented contraction and a second episode of E–W-oriented contraction (Figure 13a–b). This is further illustrated by the oval shape of several kilometers wide fold structures in map view, showing short N–S axes and elongated E–W axes (Figure 8). The unsuitable (sub-) orthogonal orientation of E–W folds and thrusts (Figure 13a) to the second episode of E–W-oriented contraction (Figure 13b) likely offered high resistance to deformation and tectonic reworking, hence resulting in gentler and less evolved geometries for N–S-trending folds, and in the shorter N–S-trending axis of the dome-shaped folds (Figure 8). Reworking and tightening of E–W folds and thrusts is also supported by the abnormally steep dip of the thrusts and by isoclinal and recumbent fold geometries (Figures 2, 4, and 6d–e). Alternatively, the second episode of E–W-oriented contraction was less intense than the first episode of N–S-oriented contraction, thus possibly resulting into less evolved geometries.

The reworked character of E–W to WNW–ESE structures is further illustrated by the geometry of the main shear zone. In N–S cross section, the shear zone dips consistently towards the north-northeast and shows a relatively planar geometry (Figure 6a–c), whereas it displays an east-dipping and upwards-convex geometry in E–W cross section (Figures 7, 9a, and 13). This geometry is analogous to that of the dome-shaped folds and suggests that the initially NNE-dipping shear zone was later deformed into a N–S-trending, north-plunging fold structure, which now forms a warp at the top of the western Selis
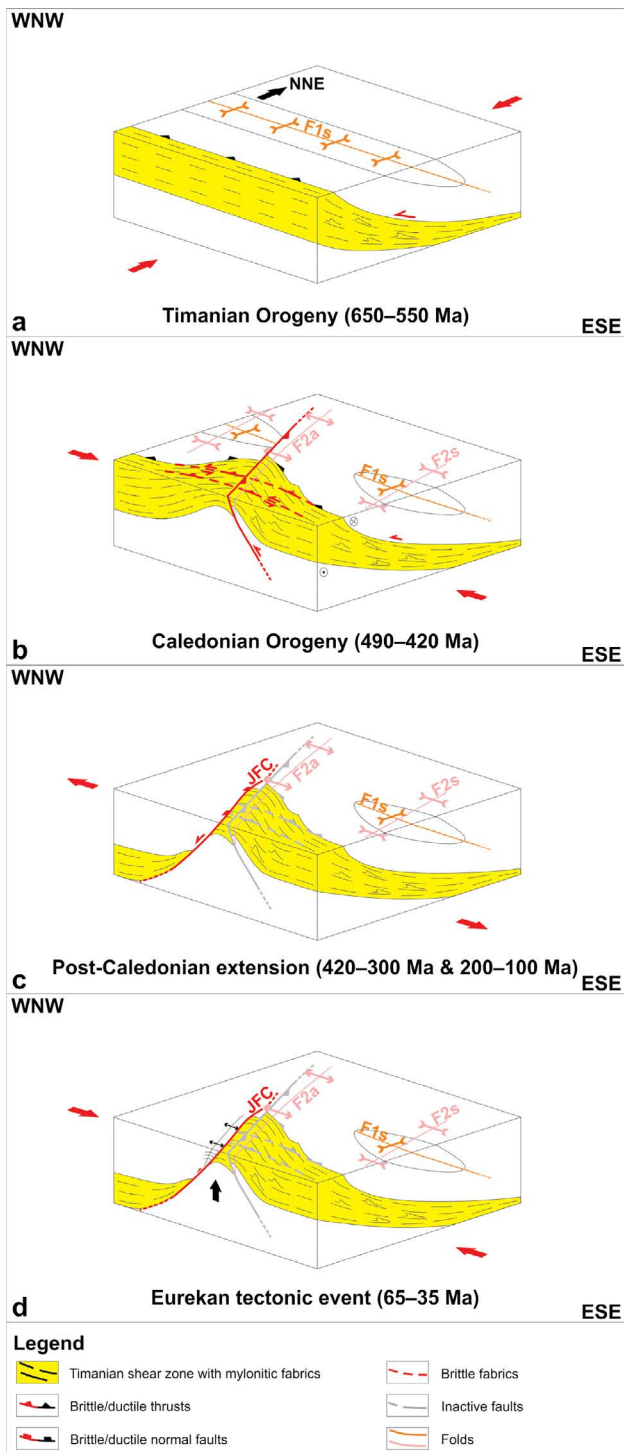
Figure 13 – Tectonic evolution of the Timanian thrust system in the Selis Ridge. **(a)** Top-SSW thrusting and associated F1 folding. Notice the formation of SSW-verging folds within the shear zone. **(b)** Caledonian reworking of major shear zones and of F1 folds into N–S-trending folds (F2) and top-west thrusting. Notice the formation of west-verging folds within the reactivated shear zone. **(c)** Post-Caledonian (Carboniferous–Permian and Jurassic–Cretaceous) extension leading to the formation of the Jason Fault Complex along the western limb of the N–S-folded major shear zone and, eventually, to the down-west truncation of the shear zone. **(d)** Eurekan inversion of the Jason Fault Complex and uplift of the Selis Ridge. Abbreviations: F1s: F1 synform; F2a: F2 antiform; F2s: F2 synform; JFC: Jason Fault Complex.

Ridge (Figures 7 and 9a).

5.2 Timing of Formation

Two pre-Devonian events fitting the inferred cross-cutting relationships and main tectonic stress orientation are the Timanian and Caledonian orogenies. The former led to the formation of WNW–ESE, dominantly top-SSW folds and thrusts in northwestern Russia (*Siedlecka and Roberts*, 1995; *Olovyanishnikov et al.*, 2000; *Lorenz et al.*, 2004; *Roberts et al.*, 2004; *Korago et al.*, 2004; *Kostyuchenko et al.*, 2006), northern Norway (*Siedlecka and Siedlecki*, 1967, 1971; *Siedlecka*, 1975), and Svalbard and the northern Barents Sea (*Manecki et al.*, 1998; *Majka et al.*, 2008; *Mazur et al.*, 2009; *Klitzke et al.*, 2019; *Faehnrich et al.*, 2020; *Koehl*, 2020; *Koehl et al.*, 2022a; *Koglin et al.*, 2022), through NNE–SSW-oriented contraction. The latter resulted into NE–SW- and N–S-trending structures respectively in northern Norway (*Ramsay et al.*, 1985; *Townsend et al.*, 1986; *Gayer et al.*, 1987; *Townsend*, 1987; *Kirkland et al.*, 2007b) and Svalbard (*Horsfield*, 1972; *Birkenmajer*, 1975, 2004; *Harland*, 1978; *Manby*, 1986; *Ohta et al.*, 1989, 1995; *Dallmeyer et al.*, 1990; *Harland et al.*, 1992; *Gee and Page*, 1994; *Gee et al.*, 1994; *Lyberis and Manby*, 1999; *Johansson et al.*, 2004, 2005), with a documented switch of trend on the Finnmark Platform and the Bjarmeland Platform (*Gernigon and Brönner*, 2012; *Gernigon et al.*, 2014).

The switch of trend occurs south of the Selis Ridge, which suggests that the N–S-trending folds and thrusts in the study area are probably Caledonian. The west-verging character of N–S folds and thrust in the Selis Ridge is consistent with the top-west vergence and transport direction of Caledonian structures in Bjørnøya (*Braathen et al.*, 1999) and northeastern Svalbard (*Flood et al.*, 1969; *Harland et al.*, 1992; *Gee and Page*, 1994; *Lyberis and Manby*, 1999). Note that the geometry of N–S-trending symmetric folds within the west-verging fold-and-thrust system in the Selis Ridge (Figure 7 and Figure SI-1 in Supporting Information) is comparable to that of Caledonian folds in basement rocks in Svalbard and the northern Barents Sea (*Koehl and Allaart*, 2021; *Koehl et al.*, 2022a).

The system of E–W folds and thrusts is sub-parallel to WNW–ESE-striking Timanian structures in Russia (e.g., Central Timan and West Timan faults and Baidaratsky Fault Zone; *Olovyanishnikov et al.*, 2000; *Lopatin et al.*, 2001; *Korago et al.*, 2004; *Roberts et al.*, 2004; *Lorenz et al.*, 2004; *Kostyuchenko et al.*, 2006), northern Norway (e.g., Trollfjorden–Komagelva Fault Zone; *Siedlecka and Siedlecki*, 1967, 1971; *Siedlecka*, 1975) and Svalbard (e.g., Vimsodden–Kosibapasset Shear Zone; *Mazur et al.*, 2009; *Faehnrich et al.*, 2020). The subtle difference in trend potentially reflects mild Caledonian reworking, e.g., folding in map view. Such map-view folding was recently reported for Timanian folds and thrusts in the northwestern Barents Sea near the Caledonian collision zone, where they alternate between E–W and NW–SE orientations (*Kl-*

itzke et al., 2019; Koehl, 2020; Koehl et al., 2022a). Therefore, we propose that the E–W-trending fold-and-thrust system in the Selis Ridge represents the reworked portion of a Timanian thrust system (Figure 13a). This is further supported by their top-SSW transport direction (Figure 6a–c), i.e., similar to the top-SSW vergence of Timanian folds and thrusts elsewhere. In addition, if originally oriented WNW–ESE like in northwestern Russia, northern Norway and the eastern Barents Sea, Timanian faults in the Selis Ridge would have been ideally oriented to the main E–W Caledonian contraction to reactivate as sinistral strike-slip faults (Figure 13b). Caledonian reactivation of Timanian thrusts as sinistral strike-slip faults is documented by minor left-lateral offsets of dome-shaped folds along E–W-faults in map view (Figure 8). This suggests that deep, NW–SE-trending structures in the area, e.g., the North Loppa High Shear Zone (Gernigon and Brönner, 2012; Gernigon et al., 2014), which coincides with the northern termination of the Selis Ridge, may have also formed during the Timanian Orogeny.

Since no geochronological ages are available offshore, it is possible that E–W folds and thrusts in the Selis Ridge are Caledonian. However, they are perpendicular to the main Caledonian trend in the Barents Sea (Gernigon and Brönner, 2012; Gernigon et al., 2014), Bjørnøya (Braathen et al., 1999) and Svalbard (Horsfield, 1972; Birkenmajer, 1975, 2004; Harland, 1978; Manby, 1986; Ohta et al., 1989, 1995; Dallmeyer et al., 1990; Harland et al., 1992; Gee and Page, 1994; Gee et al., 1994; Lyberis and Manby, 1999; Johansson et al., 2004, 2005), and their reworked character suggests that they are older than N–S-trending Caledonian structures. In addition, if E–W folds and thrusts were Caledonian in age, comparable structures would probably be found in Svalbard. But despite being reactivated–overprinted during the Caledonian Orogeny, WNW–ESE-striking structures in Svalbard clearly preserve a latest Neoproterozoic (Timanian) initial signal (Manecki et al., 1998; Majka et al., 2008; Faehnrich et al., 2020; Koglin et al., 2022). Therefore, E–W-trending fold-and-thrust system in the Selis Ridge most likely formed in the latest Neoproterozoic. The mild reworking of basement rocks in the Selis Ridge during Caledonian contraction may be explained by the existence of unsuitably oriented structures and fabrics that stroke sub-parallel to the main, E–W-oriented Caledonian stress, making basement rocks in the area unlikely to be further intensely deformed.

The potential piggyback basins below the main post-Caledonian unconformity in the east and in the southern part of the ridge are separated from underlying moderately folded basement by folded erosional unconformities, which truncate underlying, moderately to tightly folded reflections at a high angle (Figures 9b–d and 10b–c). This relationship and the tighter character of fold structures within underlying basement rocks compared to those in the piggyback basins suggest that underlying basement rocks were already (partly) folded before being eroded prior to the formation of the basins. The piggyback basins therefore probably formed during the Timanian Orogeny. This is further supported by their involvement in trough-shaped folds (i.e., folded both during the Timanian and Caledonian orogenies).

5.3 Influence on post-Caledonian Faults and Basins and Reactivation–Overprinting

5.3.1 Fold Structures

The western Barents Sea–Svalbard margin was affected by early Cenozoic Eurekan contraction (Dallmann et al., 1993; Bergh and Grogan, 2003; Lasabuda et al., 2018). Therefore, we propose that the E–W- and N–S-trending folds in upper Paleozoic–lower Cenozoic sedimentary rocks and along the Bjørnøyrenna and Jason fault complexes formed during this event (Figure 13c–d). These folds affect the base of the Carboniferous–Permian succession and the main post-Caledonian unconformity and underlying basement rocks (Figure 11). However, based on the present dataset, it is uncertain to which extent basement rocks are affected by Eurekan folding since intra-basement reflections below the Bjørnøyrenna and Jason fault complexes are low amplitude and partly chaotic (Figures 7 and 11). Nonetheless, based on folding of the main post-Caledonian unconformity, basement rocks must be involved to at least the same extent as the lower part of Carboniferous–Permian succession and, therefore, deformed into an open, E–W-trending syncline (Figure 11).

N–S-trending faults and fabrics in the Selis Ridge parallel Eurekan basins and highs in the northwestern Barents Sea (Bergh and Grogan, 2003) and western Spitsbergen (Dallmann et al., 1993). The erosional truncation of Triassic sedimentary strata (especially in the western part), the absence of Jurassic–Cretaceous sediments, and the thinned Cenozoic sedimentary strata over the Selis Ridge (e.g., Indrevær et al., 2017) suggest that the ridge was uplifted in the early Cenozoic (Figure 13d). This is also supported by Late Cretaceous–early Cenozoic inversion of post-Caledonian fault boundarie (Bjørnøyrenna and Jason fault complexes; Gabrielsen et al., 1997; Indrevær et al., 2017). Nevertheless, since post-Caledonian sedimentary strata deposited over the Selis Ridge are relatively undeformed, Eurekan contraction probably had a minor impact on basement structures in the core of the Selis Ridge, which is consistent with the location of the study area some distance from the main Eurekan orogenic system in western Spitsbergen (Steel et al., 1985; Dallmann et al., 1993) and the northwestern Barents Sea (Bergh and Grogan, 2003).

5.3.2 Bjørnøyrenna and Jason Fault Complexes

The normal offset of the Base Triassic reflection, E–W-trending contractional folds, and truncation of these

folds by the Upper Regional Unconformity suggest that the Bjørnøyrenna Fault Complex formed as a normal fault sometime in the Jurassic–Early Cretaceous and was inverted during (Late Cretaceous?–) early Cenozoic Eurekan contraction. This is comparable to what was proposed by previous works (*Rønnevik and Jacobsen*, 1984; *Gabrielsen et al.*, 1990, 1997).

By contrast, wedges of thickened upper Paleozoic sedimentary rocks in the hanging wall of the Jason Fault Complex (*Indrevær et al.*, 2017) and related faults in the west (Figure 12) suggest that they initiated as normal faults in the Carboniferous–Permian (Figure 13c). Rotated fault blocks farther west with thickened wedges of Jurassic–Cretaceous sedimentary strata indicate that these faults were reactivated in the Jurassic–Cretaceous (*Indrevær et al.*, 2017, 2018). Fold structures and minor sub-vertical reverse faults in upper Paleozoic–Mesozoic sedimentary rocks in the hanging wall of the faults (*Indrevær et al.*, 2017, 2018, Figure 7) suggest they were inverted during Eurekan contraction (Figure 13d).

The exploitative and merging relationships of post-Caledonian brittle faults respectively with underlying (mylonitic?) basement fabrics and with basement-seated folds in the study area further highlight the strong influence of preexisting fabrics and structures on subsequent faults and basins (Figures 7, 11, and 12).

5.4 Comparison with Timanian and Caledonian Structures in the Northern Barents Sea

5.4.1 Timanian Structures

Notable similarities between Timanian structures in the Selis Ridge and in the northern Barents Sea and Svalbard include a dominant south-southwest vergence of main faults and folds (Figures 5 and 6a–c). In addition, the 40–50 km width of the potential Timanian fold-and-thrust system in the Selis Ridge is comparable to that of Timanian thrust systems in the northern Barents Sea and Svalbard, e.g., Kongsfjorden–Cowanodden and Kinnhøgda–Daudbjørnpynten fault zones (*Koehl et al.*, 2022a). However, E–W folds in the Selis Ridge are tighter (isoclinal; Figures 2, 4, and 6d–e) than those mapped in the northern Barents Sea (*Koehl*, 2020; *Koehl et al.*, 2022a). A possible explanation may be that these were intensely reworked during Caledonian contraction.

Timanian thrusts in the Selis Ridge show a similar reactivation and overprinting history as those in the northern Barents Sea and Svalbard. They were reactivated during Caledonian contraction as sinistral strike-slip faults, e.g., Vimsodden–Kosibapasset Shear Zone in southern Spitsbergen (*Mazur et al.*, 2009; *Faehnrich et al.*, 2020) and minor left-lateral offsets of dome-shaped folds in the Selis Ridge (Figure 8). Timanian faults in the northern Barents Sea and Svalbard were further reactivated as and overprinted by oblique-slip normal-sinistral faults in the

Devonian–Carboniferous (*Ziemniak et al.*, 2020; *Koehl*, 2020; *Koehl et al.*, 2022a) and as reverse faults near the Eurekan collision margin in the early Cenozoic (*Koehl et al.*, 2022a). This is also possibly the case for Timanian thrusts and folds in the Selis Ridge as documented by minor, moderately dipping, Carboniferous normal faults in the north and east, which developed along embrittled mylonitic surfaces and fabrics in basement rocks (Figures 11 and 12) and by probable Eurekan folding (tightening) of Timanian folds in basement rocks below the Bjørnøyrenna Fault Complex (Figure 11).

A potential partial limitation in comparing E–W folds and thrusts in the Selis Ridge with their counterparts in the northern Barents Sea and Svalbard is that 3D seismic data in the Selis Ridge only penetrate down to 3.5 seconds (TWT), whereas 2D seismic in the northern Barents Sea show depths down to 6–7 seconds (TWT; *Koehl*, 2020; *Koehl et al.*, 2022a). Thus, the portion of the newly presented, E–W-trending fold-and-thrust system in the Selis Ridge may represent the upper part of a several to tens of kilometers thick thrust system.

The folded geometry of Timanian thrust systems in the northern Barents Sea and Svalbard in map view, which consist of alternating E–W- and NW–SE-striking segments (*Klitzke et al.*, 2019; *Koehl*, 2020; *Koehl et al.*, 2022a), may have implications for structures in the southern Barents Sea, such as the Swaen Graben (*Gabrielsen et al.*, 1990; *Omosanya et al.*, 2017). The peculiar shape of the Swaen Graben mimics folded Timanian thrust systems in the northern Barents Sea and Svalbard suggesting that the E–W to NW–SE structures observed within the Selis Ridge continue eastwards below upper Paleozoic–Cenozoic sedimentary successions, thus potentially exerting structural control on the formation of post-Caledonian basins and faults there too.

5.4.2 Caledonian Structures

In the northern Barents Sea, hundreds of meter- to several kilometer-wide, N–S-trending folds rework E–W- to WNW–ESE-trending Timanian fabrics and structures and are truncated by major post-Caledonian unconformities (*Koehl*, 2022; *Koehl et al.*, 2022a). These structures are comparable in trend/strike, size (hundreds of meters to 10 km wide; see *Koehl et al.*, 2022a, their figures 3b and 4f), and geometries to those in the Selis Ridge and, in places, they extend onshore Svalbard (*Horsfield*, 1972; *Birkenmajer*, 1975, 2004; *Harland*, 1978; *Manby*, 1986; *Ohta et al.*, 1989; *Dallmeyer et al.*, 1990; *Harland et al.*, 1992; *Gee and Page*, 1994; *Gee et al.*, 1994; *Lyberis and Manby*, 1999; *Johansson et al.*, 2004, 2005) and correspond to Caledonian folds in Proterozoic and lower Paleozoic rocks.

5.5 Implications for Late Neoproterozoic–Paleozoic Reconstructions

The present results suggest that the Caledonian suture must be located west of the Selis Ridge and of the Loppa High, and that basement rocks in the Selis Ridge are (para-) uchthonous of Baltica. This is consistent with recent work in the northern Barents Sea and Svalbard, which documented the presence of continuous WNW–ESE-striking, Timanian fold-and-thrust systems (*Koehl et al.*, 2022a), thus rejecting the inferred location of the Caledonian suture by *Breivik et al.* (2005) and placing it west of or in western Spitsbergen where blueschist- and eclogite-facies metamorphism of Caledonian age was recorded (*Horsfield*, 1972; *Dallmeyer et al.*, 1990; *Ohta et al.*, 1995; *Kośmińska et al.*, 2014), and west or in the western part of the Stappen High. This indicates that the Barents Sea block was already accreted to northern Norway in the latest Neoproterozoic.

5.6 Implications for the Location of the Timanian Suture

Island-arc magmatic suites (*Remizov*, 2003; *Remizov and Pease*, 2004) and blueschist-facies metamorphism in the Urals (*Beckholmen and Glodny*, 2004) and subduction-related granitoids (*Gee et al.*, 2000; *Pease et al.*, 2004) and mafic arc magmatism beneath the Pechora Basin (Dovzhikova et al., 2004) possibly indicate subduction beneath Baltica in the latest Neoproterozoic terminating with the Timanian Orogeny. *Pease et al.* (2004) suggested that the main Timanian suture is located between the Pechora and the Timan Range (Figure 1) based on marked changes in basement signature on gravimetric and magnetic data across the Izhma zone (*Kostyuchenko et al.*, 2006). This is supported by the presence of Timanian thrust systems both in the field and on seismic data, e.g., the East and Central Timan faults, the latter of which merges with the West Timan Fault and the Trollfjorden–Komagelva Fault Zone farther west (*Olovyanishnikov et al.*, 2000; *Lorenz et al.*, 2004; *Roberts et al.*, 2004; *Kostyuchenko et al.*, 2006, Figure 7). Regional correlation of magnetic and gravimetric anomalies related to Timanian grain and structures across the Barents Sea (*Koehl et al.*, 2022a) suggests that the western continuation of the Timanian suture near the Central and East Timan faults in the Timan Range would be located between the southernmost Selis Ridge and the western continuation of the Trollfjorden–Komagelva Fault Zone offshore, the Sørøya–Ingøya shear zone (*Koehl et al.*, 2018). This is supported by the presence of strongly foliated (pre-Caledonian?), mafic, metaigneous rocks (fine-grained gabbro/basalt?) penetrated by well 7120/1-1 in the southernmost Selis Ridge (cf. completion report of well 7120/1-1 at npd.no). However, it is also possible that foliated mafic rocks on the Selis Ridge are related to the Seiland Igneous Province. Future studies of basement rocks and crosscutting structures in the Loppa High, Finnmark Platform, and below the Hammerfest Basin will hopefully provide more input to this outstanding question.

6 Conclusions

1. The Selis Ridge is transected by a 40–50 km wide, several kilometers thick, E–W-trending, latest Neoproterozoic, Timanian fold-and-thrust system, including a NNE-dipping shear zone (and possibly shear-zone-parallel intrusions), which was mildly reworked into dome-shaped structures by a less-developed 10–20 km wide, N–S-trending system of west-verging Caledonian folds and thrusts in the early–mid Paleozoic.

2. The formation of post-Caledonian brittle faults on the Selis Ridge was controlled by preexisting Timanian and Caledonian folds and thrusts, as shown by exploitative and merging relationships.

3. The Caledonian suture is located west of the Selis Ridge.

4. Basement rocks of the Selis Ridge were already accreted to Baltica in the latest Neoproterozoic.

5. The Timanian suture in the western Barents Sea is probably located on the southernmost edge of the Selis Ridge or below the Hammerfest Basin.

Acknowledgements

Author contributions

JBPK wrote the manuscript and interpreted the data (contribution: 40%). **IP** and **LR** processed the data, and provided critical input on the manuscript writing and data interpretation and wrote the method chapter (contribution: 30% each).

Data availability

The 3D seismic data and the results of exploration wells 7220/6-1 and 7220/6-2 R are the property of Lundin Energy Norway and can therefore not be shared. High-resolution versions of the figures are available on DataverseNo at https://-doi.org/10.18710/GID9XB. See Supporting Information for additional material (https://tektonika.online/index.php/home/article/view/9/15).

Competing interests

The authors declare no competing interests.

Peer review

This publication was peer-reviewed by Laurent Gernigon and Roy Gabrielsen. The full peer-review report can be found here: https://tektonika.online/index.php/home/article/view/9/16

Copyright notice

© Author(s) 2023. This article is distributed under the Creative Commons Attribution 4.0 International License, which permits unrestricted use, distribution, and reproduction in any medium, provided the original author(s) and source are credited, and any changes made are indicated.

References

Aakvik, R. (1981), Fasies analyse av undre karbonske kullførende sedimenter, billefjorden, spitsbergen, Ph.D. thesis, University of Bergen, Bergen, Norway.

Ahlborn, M., and L. Stemmerik (2015), Depositional evolution of the upper carboniferous – lower permian wordiekammen carbonate platform, nordfjorden high, central spitsbergen, arctic norway, *Norwegian Journal of Geology*, doi: 10.17850/njg95-1-03.

Anell, I., A. Braathen, S. Olaussen, and P. T. Osmundsen (2013), Evidence of faulting contradicts a quiescent northern barents shelf during the triassic, *First Break*, *31*(6), doi: 10.3997/1365-2397.2013017.

Anell, I., J.-I. Faleide, and A. Braathen (2016), Regional tectono-sedimentary development of the highs and basins of the northwestern barents shelf, *Norwegian Journal of Geology*, doi: 10.17850/njg96-1-04.

Arbaret, L., and J.-P. Burg (2003), Complex flow in lowest crustal, anastomosing mylonites: Strain gradients in a kohistan gabbro, northern pakistan, *Journal of geophysical research*, *108*(B10), doi: 10.1029/2002jb002295.

Beckholmen, M., and J. Glodny (2004), Timanian blueschist-facies metamorphism in the kvarkush metamorphic basement, northern urals, russia, *Geological Society, London, Memoirs*, *30*(1), 125–134, doi: 10.1144/GSL.MEM.2004.030.01.11.

Bell, T. H., and M. A. Etheridge (1973), Microstructure of mylonites and their descriptive terminology, *Lithos*, *6*(4), 337–348, doi: 10.1016/0024-4937(73)90052-2.

Bergh, S. G., and P. Grogan (2003), Tertiary structure of the Sørkapp-Hornsund region, south spitsbergen, and implications for the offshore southern extension of the fold-thrust belt, *Norwegian Journal of Geology/Norsk Geologisk Forening*, *83*(1).

Birkenmajer, K. (1975), Caledonides of svalbard and plate tectonics, *Bulletin of the Geological Society of Denmark*, *24*(1-2), 1–19.

Birkenmajer, K. (1991), The jarlsbergian unconformity (Proterozoic/Cambrian boundary) and the problem of varangian tillites in south spitsbergen, *Polish Polar Research*.

Birkenmajer, K. (2004), Caledonian basement in NW wedel jarlsberg land south of bellsund, spitsbergen, *Polish Polar Research*.

Bjørnerud, M. (1990), An upper proterozoic unconformity in northern wedel jarlsberg land, southwest spitsbergen: lithostratigraphy and tectonic implications, *Polar research*, *8*(2), 127–139, doi: 10.3402/polar.v8i2.6809.

Bjørnerud, M., P. L. Decker, and C. Craddock (1991), Reconsidering caledonian deformation in southwest spitsbergen, *Tectonics*, *10*(1), 171–190, doi: 10.1029/90tc02396.

Boyer, S. E., and D. Elliott (1982), Thrust systems, *AAPG bulletin*, *66*, doi: 10.1306/03b5a77d-16d1-11d7-8645000102c1865d.

Braathen, A., H. D. Maher, T. E. Haabet, S. E. Kristensen, B. O. Tørudbakken, and D. Worsley (1999), Caledonian thrusting on bj rn ya: Implications for palaeozoic and mesozoic tectonism of the western barents shelf, *Norsk Geologisk Tidsskrift*, *79*(1), 57–68, doi: 10.1080/002919699433915.

Braathen, A., K. Bælum, H. Maher, Jr, and S. J. Buckley (2011), Growth of extensional faults and folds during deposition of an evaporite-dominated half-graben basin; the carboniferous billefjorden trough, svalbard, *Norwegian Journal of Geology*, *91*(3), 137–160.

Braathen, A., P. T. Osmundsen, H. Maher, and M. Ganerød (2018), The keisarhjelmen detachment records Silurian-Devonian extensional collapse in northern svalbard, *Terra nova*, *30*(1), 34–39, doi: 10.1111/ter.12305.

Breivik, A. J., R. Mjelde, P. Grogan, H. Shimamura, Y. Murai, and Y. Nishimura (2005), Caledonide development offshore–onshore svalbard based on ocean bottom seismometer, conventional seismic, and potential field data, *Tectonophysics*, *401*(1), 79–117, doi: 10.1016/j.tecto.2005.03.009.

Chalmers, J. A., and T. C. R. Pulvertaft (2001), Development of the continental margins of the labrador sea: a review, *Geological Society, London, Special Publications*, *187*(1), 77–105, doi: 10.1144/GSL.SP.2001.187.01.05.

Chauvet, A., and M. Séranne (1994), Extension-parallel folding in the scandinavian caledonides: Implications for late-orogenic processes, *Tectonophysics*, *238*(1), 31–54, doi: 10.1016/0040-1951(94)90048-5.

Christensen, N. I. (1965), Compressional wave velocities in metamorphic rocks at pressures to 10 kilobars, *Journal of geophysical research*, *70*(24), 6147–6164, doi: 10.1029/jz070i024p06147.

Christensen, N. I. (1966), Shear wave velocities in metamorphic rocks at pressures to 10 kilobars, *Journal of geophysical research*, *71*(14), 3549–3556, doi: 10.1029/jz071i014p03549.

Christensen, N. I., and D. L. Szymanski (1988), Origin of reflections from the brevard fault zone, *Journal of geophysical research*, *93*(B2), 1087, doi: 10.1029/jb093ib02p01087.

Clerc, C., J.-C. Ringenbach, L. Jolivet, and J.-F. Ballard (2018), Rifted margins: Ductile deformation, boudinage, continentward-dipping normal faults and the role of the weak lower crust, *Gondwana Research*, *53*, 20–40, doi: 10.1016/j.gr.2017.04.030.

Corfu, F., R. J. Roberts, T. H. Torsvik, L. D. Ashwal, and D. M. Ramsay (2007), Peri-Gondwanan elements in the caledonian nappes of finnmark, northern norway: Implications for the paleogeographic framework of the scandinavian caledonides, *American journal of science*, *307*(2), 434–458, doi: 10.2475/02.2007.05.

Cutbill, J. L., and A. Challinor (1965), Revision of the stratigraphical scheme for the carboniferous and permian rocks of spitsbergen and bjørnøya, *Geological magazine*, *102*(5), 418–439, doi: 10.1017/S0016756800053693.

Cutbill, J. L., W. G. Henderson, and N. J. R. Wright (1976), The billefjorden group (early carboniferous) of central spitsbergen, *Norsk Polarinstitutt Skrifter*, *164*, 57–89.

Dallmann, W. K., A. Andresen, S. G. Bergh, H. D. Maher, Jr, and Y. Ohta (1993), Tertiary fold-and-thrust belt of spitsbergen, svalbard, *Norsk Polarinstitutt Meddelelser*.

Dallmeyer, R. D., J. J. Peucat, T. Hirajima, and Y. Ohta (1990), Tectonothermal chronology within a blueschisteclogite complex, west-central spitsbergen, svalbard: Evidence from 40Ar39Ar and RbSr mineral ages, *Lithos*, *24*(4), 291–304, doi: 10.1016/0024-4937(89)90049-2.

Dovzhikova, E., V. Pease, and D. Remizov (2004), Neoproterozoic island are magmatism beneath the pechora basin, NW russia, *GFF*, *126*(4), 353–362, doi: 10.1080/11035890401264353.

Dumais, M.-A., L. Gernigon, O. Olesen, S. E. Johansen, and M. Brönner (2020), New interpretation of the spreading evolution of the knipovich ridge derived from aeromagnetic data, *Geophysical Journal International*, *224*(2), 1422–1428, doi: 10.1093/gji/ggaa527.

Eberts, A., H. Fazlikhani, W. Bauer, H. Stollhofen, H. de Wall, and G. Gabriel (2021), Late to post-variscan basement segmentation and differential exhumation along the SW bohemian massif, central europe, *Solid earth*, *12*(10), 2277–2301, doi: 10.5194/se-12-2277-2021.

Estrada, S., F. Tessensohn, and B.-L. Sonntag (2018a), A timanian island-arc fragment in north greenland: The midtkap igneous suite, *Journal of Geodynamics*, *118*, 140–153, doi: 10.1016/j.jog.2018.01.015.

Estrada, S., K. Mende, A. Gerdes, A. Gärtner, M. Hofmann, C. Spiegel, D. Damaske, and N. Koglin (2018b), Proterozoic to cretaceous evolution of the western and central pearya terrane (canadian high arctic), *Journal of Geodynamics*, *120*, 45–76, doi: 10.1016/j.jog.2018.05.010.

Faehnrich, K., J. Majka, D. Schneider, S. Mazur, M. Manecki, G. Ziemniak, V. T. Wala, and J. V. Strauss (2020), Geochronological constraints on caledonian strike–slip displacement in svalbard, with implications for the evolution of the arctic, *Terra nova*, *32*(4), 290–299, doi: 10.1111/ter.12461.

Faleide, J. I., S. T. Gudlaugsson, and G. Jacquart (1984), Evolution of the western barents sea, *Marine and Petroleum Geology*, *1*(2), 123–150, doi: 10.1016/0264-8172(84)90082-5.

Faleide, J. I., E. Vågnes, and S. T. Gudlaugsson (1993), Late Mesozoic-Cenozoic evolution of the south-western barents sea in a regional rift-shear tectonic setting, *Marine and Petroleum Geology*, *10*(3), 186–214, doi: 10.1016/0264-8172(93)90104-Z.

Faleide, J. I., F. Tsikalas, A. J. Breivik, R. Mjelde, O. Ritzmann, Ø. Engen, J. Wilson, and O. Eldholm (2008), Structure and evolution of the continental margin off norway and the barents sea, *Episodes*, *31*(1), 82–91, doi: 10.18814/epiiugs/2008/v31i1/012.

Fazli Khani, H., H. Fossen, R. L. Gawthorpe, J. L. Faleide, and R. E. Bell (2017), Basement structure and its influence on the structural configuration of the northern north sea, *Tectonics*, doi: 10.1002/2017TC004514.

Fichler, C., and Z. Pastore (2022), Petrology of the crystalline crust in the southwestern barents sea inferred from geophysical data, *Norwegian Journal of Geology*, doi: 10.17850/njg102-2-2.

Fisher, M. A., T. M. Brocher, W. J. Nokleberg, G. Plafker, and G. L. Smith (1989), Seismic reflection images of the crust of the northern part of the chugach terrane, alaska: Results of a survey for the Trans-Alaska crustal transect (TACT), *Journal of geophysical research*, *94*(B4), 4424–4440, doi: 10.1029/jb094ib04p04424.

Flood, B., D. G. Gee, A. Hjelle, T. Siggerud, and T. S. Winsnes (1969), The geology of nordaustlandet, northern and central parts, *Tech. rep.*, Norsk Polarinstitutt Skrifter.

Fountain, D. M., C. A. Hurich, and S. B. Smithson (1984), Seismic reflectivity of mylonite zones in the crust, *Geology*, *12*(4), 195–198, doi: 10.1130/0091-7613(1984)12<195:SROMZI>2.0.CO;2.

Friend, P. F., W. B. Harland, D. A. Rogers, I. Snape, and R. S. W. Thornley (1997), Late silurian and early devonian stratigraphy and probable strike-slip tectonics in northwestern spitsbergen, *Geological magazine*, *134*(4), 459–479, doi: 10.1017/S0016756897007231.

Gabrielsen, R. H. (1984), Long-lived fault zones and their influence on the tectonic development of the southwestern barents sea, *Journal of the Geological Society*, *141*(4), 651–662, doi: 10.1144/gsjgs.141.4.0651.

Gabrielsen, R. H., R. Foerseth, G. Hamar, and H. Rønnevik (1984), Nomenclature of the main structural features on the norwegian continental shelf north of the 62nd parallel, in *Petroleum Geology of the North European Margin*, pp. 41–60, Springer Netherlands, doi: 10.1007/978-94-009-5626-1_5.

Gabrielsen, R. H., R. B. Faerseth, and L. N. Jensen (1990), Structural elements of the norwegian continental shelf. pt. 1. the barents sea region, *Tech. Rep. 6*, Norwegian Petroleum Directorate.

Gabrielsen, R. H., I. Grunnaleite, and E. Rasmussen (1997), Cretaceous and tertiary inversion in the bjørnøyrenna fault complex, south-western barents sea, *Marine and Petroleum Geology*, *14*(2), 165–178, doi: 10.1016/S0264-8172(96)00064-5.

Gabrielsen, R. H., J. I. Faleide, K. A. Leever, and I. Grunnaleite (2011), Strike-slip related inversion-tectonics of the southwestern barents sea (norwegian shelf) in a plate tectonic perspective, in *Geophys. Res. Abstr.*, vol. 13.

Gabrielsen, R. H., D. Roberts, T. Gjelsvik, T. O. Sygnabere, M. Hassaan, and J. I. Faleide (2022), Double-folding and thrust-front geometries associated with the timanian and caledonian orogenies in the varanger peninsula, finnmark, north norway, *Journal of the Geological Society*, *179*(6), jgs2021–153, doi: 10.1144/jgs2021-153.

Gayer, R. A., S. J. Hayes, and A. H. N. Andrice (1985), The structural development of the kalak nappe complex of eastern and central porsangerhalvoya, finnmark, norway, *Tech. Rep. 400*, Norges geologiske undersøkelse bulletin.

Gayer, R. A., A. H. N. Rice, D. Roberts, C. Townsend, and A. Welbon (1987), Restoration of the caledonian baltoscandian margin from balanced cross-sections: the problem of excess continental crust, *Earth and environmental science transactions of the Royal Society of Edinburgh*, *78*(3), 197–217, doi: 10.1017/S026359330001110X.

Gee, D. G., and L. M. Page (1994), Caledonian terrane assembly on svalbard; new evidence from 40 ar/ 39 ar dating in ny friesland, *American journal of science*, *294*(9),

1166–1186, doi: 10.2475/ajs.294.9.1166.

Gee, D. G., L. Björklund, and L.-K. Stølen (1994), Early proterozoic basement in ny friesland—implications for the caledonian tectonics of svalbard, *Tectonophysics*, *231*(1), 171–182, doi: 10.1016/0040-1951(94)90128-7.

Gee, D. G., L. Beliakova, V. Pease, A. Larionov, and L. Dovshikova (2000), New, single zircon (pb-evaporation) ages from vendian intrusions in the basement beneath the pechora basin, northeastern baltica, *Polarforschung*, *68*, 161–170.

Gernigon, L., and M. Brönner (2012), Late Palaeozoic architecture and evolution of the southwestern Barents Sea: insights from a new generation of aeromagnetic data, *Journal of the Geological Society*, *169*(4), 449–459, doi: 10.1144/0016-76492011-131.

Gernigon, L., M. Brönner, D. Roberts, O. Olesen, A. Nasuti, and T. Yamasaki (2014), Crustal and basin evolution of the southwestern barents sea: From caledonian orogeny to continental breakup, *Tectonics*, *33*(4), 347–373, doi: 10.1002/2013tc003439.

Gernigon, L., M. Brönner, M.-A. Dumais, S. Gradmann, A. Grønlie, A. Nasuti, and D. Roberts (2018), Basement inheritance and salt structures in the SE barents sea: Insights from new potential field data, *Journal of Geodynamics*, *119*, 82–106, doi: 10.1016/j.jog.2018.03.008.

Gjelberg, J. (1984), Early-middle carboniferous sedimentation on svalbard. a study of ancient alluvial and coastal marine sedimentation in rift and strike-slip basins, Ph.D. thesis, University of Bergen, Bergen, Norway.

Griffin, W. L., N. Nikolic, S. Y. O'Reilly, and N. J. Pearson (2012), Coupling, decoupling and metasomatism: Evolution of crust–mantle relationships beneath NW spitsbergen, *Lithos*, *149*, 115–135, doi: 10.1016/j.lithos.2012.03.003.

Gudlaugsson, S. T., J. I. Faleide, S. Fanavoll, and B. Johansen (1987), Deep seismic reflection profiles across the western barents sea, *Geophysical Journal International*, *89*(1), 273–278, doi: 10.1111/j.1365-246X.1987.tb04419.x.

Gudlaugsson, S. T., J. I. Faleide, S. E. Johansen, and A. J. Breivik (1998), Late palaeozoic structural development of the south-western barents sea, *Marine and Petroleum Geology*, *15*(1), 73–102, doi: 10.1016/S0264-8172(97)00048-2.

Hajnal, Z., S. Lucas, D. White, J. Lewry, S. Bezdan, M. R. Stauffer, and M. D. Thomas (1996), Seismic reflection images of high-angle faults and linked detachments in the Trans-Hudson orogen, *Tectonics*, *15*(2), 427–439, doi: 10.1029/95tc02710.

Harland, W. B. (1978), The caledonides of svalbard, in *Caledonian – Appalachian Orogen of the North Atlantic Region*, edited by W. B. Harland, pp. 3–12, The Geological Association of Canada.

Harland, W. B., R. A. Scott, K. A. Auckland, and I. Snape (1992), The ny friesland orogen, spitsbergen, *Geological magazine*, *129*(6), 679–707, doi: 10.1017/S0016756800008438.

Hedin, P., B. Almqvist, T. Berthet, C. Juhlin, S. Buske, H. Simon, R. Giese, F. Krauß, J.-E. Rosberg, and P.-G. Alm (2016), 3D reflection seismic imaging at the 2.5km deep COSC-1 scientific borehole, central scandinavian caledonides, *Tectonophysics*, *689*, 40–55, doi: 10.1016/j.tecto.2015.12.013.

Herrevold, T., R. H. Gabrielsen, and D. Roberts (2009), Structural geology of the southeastern part of the Trollfjorden-Komagelva fault zone, varanger peninsula, finnmark, north norway, *Norwegian Journal of Geology/Norsk Geologisk Forening*, *89*(4).

Horsfield, W. T. (1972), Glaucophane schists of caledonian age from spitsbergen, *Geological magazine*, *109*(1), 29–36, doi: 10.1017/S0016756800042242.

Hossack, J. R. (1984), The geometry of listric growth faults in the devonian basins of sunnfjord, W norway, *Journal of the Geological Society*, *141*(4), 629–637, doi: 10.1144/gsjgs.141.4.0629.

Hurich, C. A., S. B. Smithson, D. M. Fountain, and M. C. Humphreys (1985), Seismic evidence of mylonite reflectivity and deep structure in the kettle dome metamorphic core complex, washington, *Geology*, *13*(8), 577–580, doi: 10.1130/0091-7613(1985)13<577:SEOMRA>2.0.CO;2.

Indrevær, K., S. G. Bergh, J.-B. Koehl, J.-A. Hansen, E. R. Schermer, and A. Ingebrigtsen (2013), Post-Caledonian brittle fault zones on the hyperextended SW barents sea margin: New insights into onshore and offshore margin architecture, *Norwegian Journal of Geology*, *93*(3-4).

Indrevær, K., R. H. Gabrielsen, and J. I. Faleide (2017), Early cretaceous synrift uplift and tectonic inversion in the loppa high area, southwestern barents sea, norwegian shelf, *Journal of the Geological Society*, *174*(2), 242–254, doi: 10.1144/jgs2016-066.

Indrevær, K., S. Gac, R. H. Gabrielsen, and J. I. Faleide (2018), Crustal-scale subsidence and uplift caused by metamorphic phase changes in the lower crust: a model for the evolution of the loppa high area, SW barents sea from late paleozoic to present, *Journal of the Geological Society*, *175*(3), 497–508, doi: 10.1144/jgs2017-063.

Jakobsson, M., L. Mayer, B. Coakley, J. A. Dowdeswell, S. Forbes, B. Fridman, H. Hodnesdal, R. Noormets, R. Pedersen, M. Rebesco, H. W. Schenke, Y. Zarayskaya, D. Accettella, A. Armstrong, R. M. Anderson, P. Bienhoff, A. Camerlenghi, I. Church, M. Edwards, J. V. Gardner, J. K. Hall, B. Hell, O. Hestvik, Y. Kristoffersen, C. Marcussen, R. Mohammad, D. Mosher, S. V. Nghiem, M. T. Pedrosa, P. G. Travaglini, and P. Weatherall (2012), The international bathymetric chart of the arctic ocean (IBCAO) version 3.0, *Geophysical research letters*, *39*(12), doi: 10.1029/2012gl052219.

Ji, S., and C. Long (2006), Seismic reflection response of folded structures and implications for the interpretation of deep seismic reflection profiles, *Journal of Structural Geology*, *28*(8), 1380–1387, doi: 10.1016/j.jsg.2006.05.003.

Johansen, S. E., T. Henningsen, E. Rundhovde, B. M. Sæther, C. Fichler, and H. G. Rueslåtten (1994), Continuation of the caledonides north of norway: seismic reflectors within the basement beneath the southern barents sea, *Marine and Petroleum Geology*, *11*(2), 190–201, doi: 10.1016/0264-8172(94)90095-7.

Johansson, Å., A. N. Larionov, D. G. Gee, Y. Ohta, A. M. Tebenkov, and S. Sandelin (2004), Grenvillian and caledonian tectono-magmatic activity in northeasternmost svalbard, *Geological Society, London, Memoirs*, *30*(1), 207–232, doi: 10.1144/GSL.MEM.2004.030.01.17.

Johansson, A., D. G. Gee, A. N. Larionov, Y. Ohta, and A. M. Tebenkov (2005), Grenvillian and caledonian evolution of eastern svalbard - a tale of two orogenies, *Terra nova*, *17*(4), 317–325, doi: 10.1111/j.1365-3121.2005.00616.x.

Kairanov, B., A. Escalona, I. Norton, and P. Abrahamson (2021), Early cretaceous evolution of the tromsø basin,

SW barents sea, norway, *Marine and Petroleum Geology*, *123*, 104,714, doi: 10.1016/j.marpetgeo.2020.104714.

Kirkland, C. L., J. S. Daly, E. A. Eide, and M. J. Whitehouse (2007a), Tectonic evolution of the arctic norwegian caledonides from a texturally- and structurally-constrained multi-isotopic (Ar-Ar, Rb-Sr, Sm-Nd, U-Pb) study, *American journal of science*, *307*(2), 459–526, doi: 10.2475/02.2007.06.

Kirkland, C. L., J. Stephen Daly, and M. J. Whitehouse (2007b), Provenance and terrane evolution of the kalak nappe complex, norwegian caledonides: Implications for neoproterozoic paleogeography and tectonics, *The Journal of geology*, *115*(1), 21–41, doi: 10.1086/509247.

Kirkland, C. L., J. S. Daly, and M. J. Whitehouse (2008), Basement–cover relationships of the kalak nappe complex, arctic norwegian caledonides and constraints on neoproterozoic terrane assembly in the north atlantic region, *Precambrian research*, *160*(3), 245–276, doi: 10.1016/j.precamres.2007.07.006.

Kleinspehn, K. L., and C. Teyssier (1992), Tectonics of the palaeogene forlandsundet basin, spitsbergen: a preliminary report, *Norsk Geologisk Tidsskrift*, *72*(1), 93–104.

Kleinspehn, K. L., and C. Teyssier (2016), Oblique rifting and the late Eocene–Oligocene demise of laurasia with inception of molloy ridge: Deformation of forlandsundet basin, svalbard, *Tectonophysics*, *693*, 363–377, doi: 10.1016/j.tecto.2016.05.010.

Klitzke, P., D. Franke, A. Ehrhardt, R. Lutz, L. Reinhardt, I. Heyde, and J. I. Faleide (2019), The paleozoic evolution of the olga basin region, northern barents sea: A link to the timanian orogeny, *Geochemistry, Geophysics, Geosystems*, *20*(2), 614–629, doi: 10.1029/2018gc007814.

Knudsen, C., D. G. Gee, S. C. Sherlock, and L. Yu (2019), Caledonian metamorphism of metasediments from franz josef land, *GFF*, *141*(4), 295–307, doi: 10.1080/11035897.2019.1622151.

Knutsen, S.-M., and K. I. Larsen (1997), The late mesozoic and cenozoic evolution of the sørvestsnaget basin: A tectonostratigraphic mirror for regional events along the southwestern barents sea margin?, *Marine and Petroleum Geology*, *14*(1), 27–54, doi: 10.1016/S0264-8172(96)00039-6.

Knutsen, S.-M., L.-J. Skjold, and P. H. Skott (1992), Palaeocene and eocene development of the tromsø basin sedimentary response to rifting and early seafloor spreading in the barents sea area, *Norsk Geologisk Tidsskrift*, *72*, 191–207.

Koehl, J.-B. (2020), Impact of timanian thrusts on the phanerozoic tectonic history of svalbard, in *EGU General Assembly 2020, Online, 4–8 May 2020*, EGU2020-2170, pp. EGU2020–2170, Copernicus Meetings, doi: 10.5194/egusphere-egu2020-2170.

Koehl, J.-B., and L. Allaart (2021), The billefjorden fault zone north of spitsbergen: a major terrane boundary?, *Polar research*, *40*, doi: 10.33265/polar.v40.7668.

Koehl, J.-B. P. (2022), Implications of timanian thrust systems in the barents sea and svalbard on the use of paleontological constraints for plate tectonics reconstructions, doi: 10.13140/RG.2.2.15321.39525.

Koehl, J.-B. P., S. G. Bergh, T. Henningsen, and J. I. Faleide (2018), Middle to late Devonian–Carboniferous collapse basins on the finnmark platform and in the southwesternmost nordkapp basin, SW barents sea, *Solid earth*, *9*(2), 341–372, doi: 10.5194/se-9-341-2018.

Koehl, J.-B. P., C. Magee, and I. M. Anell (2022a), Impact of timanian thrust systems on the late Neoproterozoic–Phanerozoic tectonic evolution of the barents sea and svalbard, *Solid earth*, *13*(1), 85–115, doi: 10.5194/se-13-85-2022.

Koehl, J.-B. P., J. E. A. Marshall, and G. Lopes (2022b), The timing of the svalbardian orogeny in svalbard: a review, *Solid Earth*, *13*(8), 1353–1370, doi: 10.5194/se-13-1353-2022.

Koglin, N., A. Läufer, K. Piepjohn, A. Gerdes, D. W. Davis, U. Linnemann, and S. Estrada (2022), Paleozoic sedimentation and caledonian terrane architecture in NW svalbard: indications from U–Pb geochronology and structural analysis, *Journal of the Geological Society*, *179*(4), jgs2021–053, doi: 10.1144/jgs2021-053.

Korago, E. A., G. N. Kovaleva, B. G. Lopatin, and V. V. Orgo (2004), The precambrian rocks of novaya zemlya, *Geological Society, London, Memoirs*, *30*(1), 135–143, doi: 10.1144/GSL.MEM.2004.030.01.12.

Kośmińska, K., J. Majka, S. Mazur, M. Krumbholz, I. Klonowska, M. Manecki, J. Czerny, and M. Dwornik (2014), Blueschist facies metamorphism in nordenskiöld land of west-central svalbard, *Terra nova*, *26*(5), 377–386, doi: 10.1111/ter.12110.

Kostyuchenko, S., R. Sapozhnikov, A. Egorkin, D. G. Gee, R. Berzin, and L. Solodilov (2006), Crustal structure and tectonic model of northeastern baltica, based on deep seismic and potential field data, *Geological Society, London, Memoirs*, *32*(1), 521–539, doi: 10.1144/GSL.MEM.2006.032.01.32.

Kristensen, T. B., A. Rotevatn, M. Marvik, G. A. Henstra, R. L. Gawthorpe, and R. Ravnås (2018), Structural evolution of sheared margin basins: the role of strain partitioning. sørvestsnaget basin, norwegian barents sea, *Basin Research*, *30*(2), 279–301, doi: 10.1111/bre.12253.

Kurapov, M., V. Ershova, A. Khudoley, A. Makariev, and E. Makarieva (2020), The first evidence of late ordovician magmatism of the october revolution island (severnaya zemlya archipelago, russian high arctic): geochronology, geochemistry and geodynamic settings, *Norwegian Journal of Geology/Norsk Geologisk Forening*, *100*(1).

Kuznetsov, N. B., A. A. Soboleva, O. V. Udoratina, M. V. Hertseva, and V. L. Andreichev (2007), Pre-Ordovician tectonic evolution and volcano–plutonic associations of the timanides and northern Pre-Uralides, northeast part of the east european craton, *Gondwana Research*, *12*(3), 305–323, doi: 10.1016/j.gr.2006.10.021.

Larionov, A. N., V. A. Andreichev, and D. G. Gee (2004), The vendian alkaline igneous suite of northern timan: ion microprobe U-Pb zircon ages of gabbros and syenite, *Geological Society, London, Memoirs*, *30*(1), 69–74, doi: 10.1144/GSL.MEM.2004.030.01.07.

Larssen, G. B. (2005), *Upper Palaeozoic Lithostratigraphy of the Southern Part of the Norwegian Barents Sea*, vol. 444, Norges geologiske undersøkelse.

Lasabuda, A., J. S. Laberg, S.-M. Knutsen, and P. Safronova (2018), Cenozoic tectonostratigraphy and pre-glacial erosion: A mass-balance study of the northwestern barents sea margin, norwegian arctic, *Journal of Geodynamics*, *119*, 149–166, doi: 10.1016/j.jog.2018.03.004.

Lenhart, A., C. A.-L. Jackson, R. E. Bell, O. B. Duffy, R. L. Gawthorpe, and H. Fossen (2019), Structural architecture and composition of crystalline basement offshore west norway, *Lithosphere*, *11*(2), 273–293, doi: 10.1130/L668.1.

Lepvrier, C. (1990), Early tertiary paleostress history and tectonic development of the forlandsundet basin, svalbard, norway, *Tech. Rep. 112*, Norsk Polarinstitutt Meddelelser.

Lopatin, B. G., L. G. Pavlov, V. V. Orgo, and S. Shkarubo (2001), Teetonic structure of novaya zemlya, *Polarforschung*, *69*, 131–135.

Lorenz, H., A. M. Pystin, V. G. Olovyanishnikov, and D. G. Gee (2004), Neoproterozoic high-grade metamorphism of the kanin peninsula, timanide orogen, northern russia, *Geological Society, London, Memoirs*, *30*(1), 59–68, doi: 10.1144/GSL.MEM.2004.030.01.06.

Lyberis, N., and G. Manby (1999), Continental collision and lateral escape deformation in the lower and upper crust: An example from caledonide svalbard, *Tectonics*, *18*(1), 40–63, doi: 10.1029/1998tc900013.

Majka, J., S. Mazur, M. Manecki, J. Czerny, and D. K. Holm (2008), Late neoproterozoic amphibolite-facies metamorphism of a pre-caledonian basement block in southwest wedel jarlsberg land, spitsbergen: new evidence from U–Th–Pb dating of monazite, *Geological magazine*, *145*(6), 822–830, doi: 10.1017/S001675680800530X.

Majka, J., A. N. Larionov, D. G. Gee, J. Czerny, and J. Pršek (2012), Neoproterozoic pegmatite from skoddefjellet, wedel jarlsberg land, spitsbergen: Additional evidence for c. 640 ma tectonothermal event in the caledonides of svalbard, *Polish Polar Research*, pp. 1–17.

Manby, G. M. (1986), Mid-Palaeozoic metamorphism and polyphase deformation of the forland complex, svalbard, *Geological magazine*, *123*(6), 651–663, doi: 10.1017/S001675680002416X.

Manecki, M., D. K. Holm, J. Czerny, and D. Lux (1998), Thermochronological evidence for late proterozoic (vendian) cooling in southwest wedel jarlsberg land, spitsbergen, *Geological magazine*, *135*(1), 63–69, doi: 10.1017/S0016756897008297.

Marín, D., S. Helleren, A. Escalona, S. Olaussen, A. Cedeño, H. Nøhr-Hansen, and S. Ohm (2021), The middle jurassic to lowermost cretaceous in the SW barents sea: Interplay between tectonics, coarse-grained sediment supply and organic matter preservation, *Basin Research*, *33*(2), 1033–1055, doi: 10.1111/bre.12504.

Matapour, Z., D. A. Karlsen, B. Lerch, and K. Backer-Owe (2019), Petroleum occurrences in the carbonate lithologies of the gohta and alta discoveries in the barents sea, arctic norway, *Petroleum Geoscience*, *25*(1), 50–70, doi: 10.1144/petgeo2017-085.

Mazur, S., J. Czerny, J. Majka, M. Manecki, D. Holm, A. Smyrak, and A. Wypych (2009), A strike-slip terrane boundary in wedel jarlsberg land, svalbard, and its bearing on correlations of SW spitsbergen with the pearya terrane and timanide belt, *Journal of the Geological Society*, *166*(3), 529–544, doi: 10.1144/0016-76492008-106.

Murascov, L. G., and J. I. Mokin (1979), Stratigraphic subdivision of the devonian deposits of spitsbergen, *Norsk Polarinstitutt Skrifter*, *167*, 249–261.

Nordaunet-Olsen, E. M., A. Escalona, T. Skar, and L. Pedersen (2015), Controls on upper paleozoic carbonate build-up development in the SC barents sea, in *3PArctic Conference*.

Norton, M. G. (1987), The Nordfjord-Sogn detachment, w. norway, *Norsk Geologisk Tidsskrift*, *67*(2), 93–106.

Nøttvedt, A., L. T. Berglund, E. Rasmussen, and R. J. Steel (1988), Some aspects of tertiary tectonics and sedimentation along the western barents shelf, *Geological Society, London, Special Publications*, *39*(1), 421–425, doi: 10.1144/GSL.SP.1988.039.01.37.

Oakey, G. N., and J. A. Chalmers (2012), A new model for the paleogene motion of greenland relative to north america: Plate reconstructions of the davis strait and nares strait regions between canada and greenland, *Journal of Geophysical Research, [Solid Earth]*, *117*(B10), doi: 10.1029/2011JB008942.

O'Brien, T. M., E. L. Miller, J. P. Benowitz, K. E. Meisling, and T. A. Dumitru (2016), Dredge samples from the chukchi borderland: Implications for paleogeographic reconstruction and tectonic evolution of the amerasia basin of the arctic, *American journal of science*, *316*(9), 873–924, doi: 10.2475/09.2016.03.

Ogata, K., M. J. Mulrooney, A. Braathen, H. Maher, P. T. Osmundsen, I. Anell, A. A. Smyrak-Sikora, and F. Balsamo (2018), Architecture, deformation style and petrophysical properties of growth fault systems: the late triassic deltaic succession of southern edgeøya (east svalbard), *Basin Research*, *30*(5), 1042–1073, doi: 10.1111/bre.12296.

Ohta, Y., R. D. Dallmeyer, and J. J. Peucat (1989), Caledonian terranes in Svalbard, in *Terranes in the Circum-Atlantic Paleozoic Orogens*, Geological Society of America, doi: 10.1130/SPE230-p1.

Ohta, Y., A. A. Krasil'šikov, C. Lepvrier, and A. M. Teben'kov (1995), Northern continuation of caledonian high-pressure metamorphic rocks in central-western spitsbergen, *Polar research*, *14*(3), 303–316, doi: 10.3402/polar.v14i3.6670.

Olovyanishnikov, V. G., D. Roberts, and A. Siedleekat (2000), Teetonics and sedimentation of the meso- to neoproterozoic Timan-Varanger belt along the northeastern margin of baltica, *Polarforschung*, *68*, 267–274.

Omosanya, K. O., I. Zervas, N. H. Mattos, T. M. Alves, S. E. Johansen, and G. Marfo (2017), Strike-Slip tectonics in the SW barents sea during north atlantic rifting (swaen graben, northern norway), *Tectonics*, *36*(11), 2422–2446, doi: 10.1002/2017tc004635.

Osagiede, E. E., A. Rotevatn, R. Gawthorpe, T. B. Kristensen, C. A.-L. Jackson, and N. Marsh (2020), Pre-existing intra-basement shear zones influence growth and geometry of non-colinear normal faults, western utsira High–Heimdal terrace, north sea, *Journal of Structural Geology*, *130*, 103,908, doi: 10.1016/j.jsg.2019.103908.

Osmundsen, P. T., A. Braathen, R. S. Rød, and I. B. Hynne (2014), Styles of normal faulting and fault-controlled sedimentation in the triassic deposits of eastern svalbard, *Norwegian Petroleum directorate Bulletin*, *10*, 61–79.

Pease, V., E. Dovzhikova, L. Beliakova, and D. G. Gee (2004), Late neoproterozoic granitoid magmatism in the basement to the pechora basin, NW russia: geochemical constraints indicate westward subduction beneath NE baltica, *Geological Society, London, Memoirs*, *30*(1), 75–85, doi: 10.1144/GSL.MEM.2004.030.01.08.

Peucat, J. J., Y. Ohta, D. G. Gee, and J. Bernard-Griffiths (1989), U–Pb, sr and nd evidence for grenvillian and latest proterozoic tectonothermal activity in the spitsbergen caledonides, arctic ocean, *Lithos*, *22*(4), 275–285, doi: 10.1016/0024-4937(89)90030-3.

Phillips, T. B., and K. J. W. McCaffrey (2019), Terrane boundary reactivation, barriers to lateral fault propagation and reactivated fabrics: Rifting across the median batholith

zone, great south basin, new zealand, *Tectonics*, *38*(11), 4027–4053, doi: 10.1029/2019tc005772.

Phillips, T. B., C. A.-L. Jackson, R. E. Bell, O. B. Duffy, and H. Fossen (2016), Reactivation of intrabasement structures during rifting: A case study from offshore southern norway, *Journal of Structural Geology*, *91*, 54–73, doi: 10.1016/j.jsg.2016.08.008.

Phillips, T. B., C. Magee, C. A.-L. Jackson, and R. E. Bell (2018), Determining the three-dimensional geometry of a dike swarm and its impact on later rift geometry using seismic reflection data, *Geology*, *46*(2), 119–122, doi: 10.1130/G39672.1.

Piepjohn, K. (2000), The Svalbardian-Ellesmerian deformation of the old red sandstone and the pre-devonian basement in NW spitsbergen (svalbard), *Geological Society, London, Special Publications*, *180*(1), 585–601, doi: 10.1144/GSL.SP.2000.180.01.31.

Rafaelsen, B., G. Elvebakk, K. Andreassen, L. Stemmerik, A. Colpaert, and T. J. Samuelsberg (2008), From detached to attached carbonate buildup complexes — 3D seismic data from the upper palaeozoic, finnmark platform, southwestern barents sea, *Sedimentary geology*, *206*(1), 17–32, doi: 10.1016/j.sedgeo.2008.03.001.

Ramsay, D. M., B. A. Sturt, Ø. Jansen, T. B. Andersen, and S. Sinha-Roy (1985), The tectonostratigraphy of western porsangerhalvøya, finnmark, north norway, in *The Caledonides Orogen – Scandinavia and Related Areas*, edited by D. G. Gee and B. A. Sturt, pp. 611–619, John Wiley & Sons Ltd.

Rekant, P., N. Sobolev, A. Portnov, B. Belyatsky, G. Dipre, A. Pakhalko, V. Kaban'kov, and I. Andreeva (2019), Basement segmentation and tectonic structure of the lomonosov ridge, arctic ocean: Insights from bedrock geochronology, *Journal of Geodynamics*, *128*, 38–54, doi: 10.1016/j.jog.2019.05.001.

Remizov, D., and V. Pease (2004), The dzela complex, polar urals, russia: a neoproterozoic island arc, *Geological Society, London, Memoirs*, *30*(1), 107–123, doi: 10.1144/GSL.MEM.2004.030.01.10.

Remizov, D. N. (2003), Metabasite basement of the voikar island arc in the polar urals, *Polarforschung*, *73*(2/3), 49–57.

Riber, L., H. Dypvik, and R. Sørlie (2015), Altered basement rocks on the utsira high and its surroundings, norwegian north sea, *Norwegian Journal of Geology*, doi: 10.17850/njg95-1-04.

Riis, F., J. Vollset, and M. Sand (1986), Tectonic development of the western margin of the barents sea and adjacent areas, in *Future Petroleum Provinces of the World*, pp. 661–675, AAPG Special Volumes.

Roberts, D. (1983), Devonian tectonic deformation in the norwegian caledonides and its regional perspectives, *Norges geologiske undersøkelse*, *380*, 85–96.

Roberts, D. (1998), Berggrunnskart Honningsvåg–Geologisk kart over norge, M 1: 250 000.

Roberts, D., A. Siedlecka, and V. G. Olovyanishnikov (2004), Neoproterozoic, passive-margin, sedimentary systems of the kanin peninsula, and northern and central timan, NW russia, *Geological Society, London, Memoirs*, *30*(1), 5–17, doi: 10.1144/GSL.MEM.2004.030.01.02.

Rønnevik, H., and H.-P. Jacobsen (1984), Structural highs and basins in the western barents sea, in *Petroleum Geology of the North European Margin*, pp. 19–32, Springer Netherlands, doi: 10.1007/978-94-009-5626-1_3.

Rosa, D., J. Majka, K. Thrane, and P. Guarnieri (2016), Evidence for timanian-age basement rocks in north greenland as documented through U-Pb zircon dating of igneous xenoliths from the midtkap volcanic centers, *Precambrian research*, *275*, 394–405, doi: 10.1016/j.precamres.2016.01.005.

Samuelsberg, T. J., G. Elvebakk, and L. Stemmerik (2003), Late palaeozoic evolution of the finnmark platform, southern norwegian barents sea, *Norwegian Journal of Geology/Norsk Geologisk Forening*, *83*(4).

Schaaf, N. W., P. T. Osmundsen, R. Van der Lelij, J. Schönenberger, O. K. Lenz, T. Redfield, and K. Senger (2021), Tectono-sedimentary evolution of the eastern forlandsundet graben, svalbard, *Norwegian Journal of Geology*, doi: 10.17850/njg100-4-4.

Sibson, R. H. (1977), Fault rocks and fault mechanisms, *Journal of the Geological Society*, *133*(3), 191–213, doi: 10.1144/gsjgs.133.3.0191.

Siedlecka, A. (1975), Late precambrian stratigraphy and structure of the north-eastern margin of the fennoscandian shield (East-Finnmark-Timan region), *Tech. Rep. 316*, Norges geologiske undersøkelse.

Siedlecka, A., and D. Roberts (1995), Report from a visit to the komi branch of the russian academy of sciences in syktyvkar, russia, and from fieldwork in the central timans, august 1995, *Tech. Rep. 95.149*, Geological Survey of Norway.

Siedlecka, A., and S. Siedlecki (1967), Some new aspects of the geology of varanger peninsula (northern norway), *Norges geologiske undersøkelse*, *247*, 288–306.

Siedlecka, A., and S. Siedlecki (1971), Late precambrian sedimentary rocks of the Tanafjord-Varangerfjord region of varanger peninsula, northern norway, in *The Caledonian Geology of Northern Norway*, edited by D. Roberts and M. Gustavson, pp. 246–294, Norges geologiske undersøkelse.

Slagstad, T., V. A. Melezhik, C. L. Kirkland, K. B. Zwaan, D. Roberts, I. M. Gorokhov, and A. E. Fallick (2006), Carbonate isotope chemostratigraphy suggests revisions to the geological history of the west finnmark caledonides, northern norway, *Journal of the Geological Society*, *163*(2), 277–289, doi: 10.1144/0016-764905-021.

Slagstad, T., C. Barrére, B. Davidsen, and R. K. Ramstad (2008), Petrophysical and thermal properties of pre-devonian basement rocks on the norwegian continental margin, *Geological Survey of Norway Bulletin*, *44*, 1–6.

Steel, R., J. Gjelberg, W. Helland-Hansen, K. Kleinspehn, A. Nøttvedt, and M. Rye-Larsen (1985), The tertiary Strike-Slip basins and orogenic belt of spitsbergen, *Society of Economic Paleontologists and Mineralogists Special Publications*, *37*, 339–359, doi: 10.2110/pec.85.37.0319.

Steltenpohl, M. G., D. Moecher, A. Andresen, J. Ball, S. Mager, and W. E. Hames (2011), The eidsfjord shear zone, Lofoten–Vesterålen, north norway: An early devonian, paleoseismogenic low-angle normal fault, *Journal of Structural Geology*, *33*(5), 1023–1043, doi: 10.1016/j.jsg.2011.01.017.

Storey, M., R. A. Duncan, and C. Tegner (2007), Timing and duration of volcanism in the north atlantic igneous province: Implications for geodynamics and links to the iceland hotspot, *Chemical geology*, *241*(3), 264–281, doi: 10.1016/j.chemgeo.2007.01.016.

Sturt, B. A., I. R. Pringle, and D. M. Ramsay (1978), The finnmarkian phase of the caledonian orogeny,

Journal of the Geological Society, *135*(6), 597–610, doi: 10.1144/gsjgs.135.6.0597.

Sund, T., O. Skarpnes, L. N. Jensen, and R. M. Larsen (1986), Tectonic development and hydrocarbon potential offshore troms, northern norway, in *Future Petroleum Provinces of the World*, vol. 131, pp. 615–627, American Association of Petroleum Geologists, doi: 10.1306/m40454c29.

Suppe, J., and D. A. Medwedeff (1990), Geometry and kinematics of fault-propagation folding, *Eclogae Geologicae Helvetiae*, *83*(3), 409–454.

Tonstad, S. A. (2018), The late paleozoic development of the ottar basin from seismic 3D interpretation, Ph.D. thesis, UiT Norges arktiske universitet, Tromsø, Norway.

Torsvik, T. H., B. A. Sturt, D. M. Ramsay, H. J. Kisch, and D. Bering (1986), The tectonic implications of solundian (upper devonian) magnetization of the devonian rocks of kvamshesten, western norway, *Earth and planetary science letters*, *80*(3), 337–347, doi: 10.1016/0012-821X(86)90115-9.

Townsend, C. (1987), Thrust transport directions and thrust sheet restoration in the caledonides of finnmark, north norway, *Journal of Structural Geology*, *9*(3), 345–352, doi: 10.1016/0191-8141(87)90057-5.

Townsend, C., D. Roberts, A. H. N. Rice, and R. A. Gayer (1986), The gaissa nappe, finnmark, north norway: an example of a deeply eroded external imbricate zone within the scandinavian caledonides, *Journal of Structural Geology*, *8*(3), 431–440, doi: 10.1016/0191-8141(86)90061-1.

Vogt, T. (1928), Den norske fjellkjedes revolusjonshistorie, *Norsk Geologisk Tidsskrift*, *10*, 97–115.

Vogt, T., and G. Horn (1941), Geology of a middle devonian cannel coal from spitsbergen, *Norsk Geologisk Tidsskrift*, *21*, 1–12.

Wang, C.-Y., D. A. Okaya, C. Ruppert, G. A. Davis, T.-S. Guo, Z. Zhong, and H.-R. Wenk (1989), Seismic reflectivity of the whipple mountain shear zone in southern california, *Journal of geophysical research*, *94*(B3), 2989–3005, doi: 10.1029/jb094ib03p02989.

Witt-Nilsson, P., D. G. Gee, and F. J. Hellman (1998), Tectonostratigraphy of the caledonian atomfjella antiform of northern ny friesland, svalbard, *Norsk Geologisk Tidsskrift*, *78*(1), 67–80.

Worsley, D., T. Agdestein, J. G. Gjelberg, K. Kirkemo, A. Mørk, I. Nilsson, S. Olaussen, R. J. Steel, and L. Stemmerik (2001), The geological evolution of bjørnøya, arctic norway: implications for the barents shelf, *Norsk Geologisk Tidsskrift*, *81*(3), 195–234.

Wrona, T., H. Fossen, I. Lecomte, C. H. Eide, and R. L. Gawthorpe (2020), Seismic expression of shear zones: Insights from 2-D point-spread-function based convolution modelling, *Journal of Structural Geology*, *140*, 104,121, doi: 10.1016/j.jsg.2020.104121.

Ziemniak, G., J. Majka, M. Manecki, K. Walczak, P. Jeanneret, S. Mazur, and K. Kośmińska (2020), Early devonian sinistral strike-slip in the caledonian basement of oscar II land advocates for escape tectonics as a major mechanism for svalbard terranes assembly, in *EGU General Assembly*, EGU2020-1044, Copernicus Meetings, doi: 10.5194/egusphere-egu2020-1044.